

A fracture mechanics framework for optimising design and inspection of offshore Wind Turbine support structures against fatigue failure

Peyman Amirafshari¹, Feargal Brennan¹, Athanasios Kolios¹

¹Department of Naval Architecture, Ocean and Marine Engineering, University of Strathclyde, Glasgow, G4 0LZ, United Kingdom

Correspondence to: Peyman Amirafshari (amirafshari.peyman@strath.ac.uk)

Abstract

Offshore Wind Turbine (OWT) support structures need to be designed against fatigue failure under cyclic aerodynamic and wave loading. The fatigue failure can be accelerated in a corrosive sea environment. Traditionally, a stress-life approach called the S-N curve method has been used for the design of structures against fatigue failure. There are a number of limitations in the S-N approach related to welded structures which can be addressed by the fracture mechanics approach. In this paper the limitations of the S-N approach related to OWT support structure are addressed, a fatigue design framework based on fracture mechanics is developed. The application of the framework to a monopile OWT support structure is demonstrated and optimisation of in-service inspection of the structure is studied. It was found that both the design of the weld joint and Non-destructive testing techniques can be optimised to reduce in-service frequency. Furthermore, probabilistic fracture mechanics as a form of risk-based design is outlined and its application to the monopile support structure is studied. The probabilistic model showed a better capability to account for NDT reliability over a range of possible crack sizes as well as providing a risk associated with the chosen inspection time which can be used in inspection cost-benefit analysis. There are a number of areas for future research, including a better estimate of fatigue stress with a time-history analysis, the application of the framework to other types of support structures such as Jackets and Tripods, and integration of risk-based optimisation with a cost-benefit analysis.

Nonculture

Symbol	Explanation
a	Flaw size
a_0	Initial flaw size
a_f	Failure flaw size
a_{cr}	Critical flaw size
a_t	Tolerable flaw size
C	Material constant in Paris-Erdogan equation
$2C$	Crack length
I_1	First inspection

J	J integral
J_e	Elastic component of J integral
ΔK	Stress intensity factor
ΔK_{th}	Threshold Stress intensity factor
K_r	The ratio of applied stress intensity factor to the fracture toughness of the component material in the Failure Assessment Diagram
$K_{elastic\ plastic}$	Elastic-plastic stress intensity factor
$K_{elastic}$	Elastic stress intensity factor
K_{max}	Maximum stress intensity factor
K_{min}	Minimum stress intensity factor
K_{mat}	Fracture toughness
$K_{critical}$	Critical Fracture toughness value
L_r	The ratio of the applied load to the load required to cause plastic collapse of the flawed section
m	Paris equation slope
N_i	Cycle increment
P_F	Probability of a fatigue crack failure
P_{SYS}	Probability of a collapse given that there is a fatigue failure in the structure
P_t	Target probability of failure
$p_{\Delta\sigma}(\Delta\sigma)$	Probability density function of stress range $\Delta\sigma$
Y	Geometry function
$\frac{da}{dN}$	Rate of crack growth to load cycles
σ	Stress at flaw
$\Delta\sigma_{eq}$	Equivalent constant amplitude stress ranges
β	Stress contribution factor
σ_{flow}	Flow stress
σ_Y	Yield stress
σ_U	Ultimate tensile stress

ε_{ref} The true strain obtained from the uniaxial tensile stress-strain curve

Abbreviations

Acronym	Explanation
DLC	Design load case
ECM	Extreme Current Model
EU	European Union
EWM	Extreme Wind Model
FAD	Failure Assessment Diagram
FAL	Failure Assessment Line
FLS	Fatigue limit state
FM	Fracture Mechanics
HAZ	Heat affected zone
LCOE	Levelized cost of electricity
LEFM	Linear Elastic Fracture Mechanics
MPI	Magnetic Particle Inspection
NDT	Non Destructive Testing
NECPs	National Energy and Climate Plans
NSS	Normal Sea State
NTM	Normal Turbulence Model
OWT	Offshore Wind Turbine
PoD	Probability of Detection
PoND	Probability of Non-Detection
QC	Quality Control
RWH	Reduced Wave Height
SLS	Serviceability limit state
S-N	Stress - Number of cycles to failure
ULS	Ultimate limit state
UT	Ultrasonic Testing

27

28 1 Introduction

29 Wind turbines are playing a key role in decarbonising world power production system. The
30 target share of energy from renewable sources in the European Union (EU) countries set out by
31 National Energy and Climate Plans (NECPs) is aimed to reach 32% by 2030 and 100% by 2050.
32 In 2018 the total share of energy from renewable sources was 18% in the EU and 16% in the
33 United Kingdom (European Environment Agency, 2019). Thanks to the commitment of
34 European countries to achieve the above targets the prospects for the offshore renewable
35 industry for further growth continues to be strong (Fraile et al., 2019).

36 Since the power production of a wind turbine is directly related to the wind velocity at the hub,
37 the developments of Offshore Wind Turbines (OWTs) are expected to grow in order to harvest
38 more power from offshore sites where wind speed is generally higher compared to the onshore.
39 Furthermore, OWTs are socially more accepted as there are concerns towards onshore wind
40 turbines about their astatic aspects, noise pollution and their risk for birds (Tavner, 2012).

41 Despite their higher wind power capacity, the biggest disadvantage of OWTs is their
42 construction and maintenance costs. Due to their remote location, their inspection and
43 maintenance are challenging and expensive. Therefore, optimising the design and maintenance
44 of these structures can decrease the Levelized cost of electricity (LCOE) (Baum et al., 2018) and
45 (Luengo and Kolios, 2015).

46 OWT support structures constantly experience cyclic stress imposed by wind turbulence and
47 wave loading which makes them prone to fatigue failure (Barltrop and Adams, 1991). The
48 fatigue damage accumulation could be further accelerated if exposed to the corrosive marine
49 environment.

50 There are two approaches for quantifying fatigue damage: The S-N (Stress vs. Number of cycles)
51 method and the Fracture Mechanics (FM) approach.

52 Standards such as IEC 61400-3 (IEC, 2009), DNVGL-ST-0126 (DNVGL, 2016a), DNVGL-ST-
53 0437 (DNVGL, 2016b) and DNVGL-RP-C203 (DNV, 2010) are commonly used for the design of
54 offshore wind turbines against fatigue failure. Current design approaches are solely based on
55 the S-N method. In this approach, the fatigue life of a structural element is determined using a
56 relevant S-N curve, recommended by one of the standards or derived from bespoke fatigue test
57 programs. Service induced stresses, contributing to fatigue damage accumulations, are
58 determined from structural analysis then a suitable joint class capable of resisting those
59 stresses is specified. Alternatively, if the joint class is known, maximum allowable fatigue
60 stresses for the intended life of the structure are determined from the relevant S-N curve
61 (Hobbacher, 2016).

62 Fatigue design of steel structures using S-N data is commonly preferred to the Fracture
63 Mechanics approach due to its simplicity (Naess, 1985). The S-N approach is also considered
64 more reliable since it is based on fatigue test compared to the Fracture Mechanics which is
65 based on calculations where additional input variables (e.g. crack growth rate, toughness, and
66 residual stress distributions) need to be considered (Anderson, 2005).

67 Despite its popularity, a number of limitations exist with the S-N data approach concerning
68 offshore wind turbine structures:

69 **Design for inspection:** Many structures are designed considering a damage-tolerant philosophy
70 where the structure is expected to tolerate certain levels of fatigue damage until the next
71 scheduled inspection (Figure 1). The expected crack size at the time of the inspection is
72 estimated using Fracture Mechanics and a suitable non-destructive testing (NDT) technique
73 capable of detecting the critical crack size is prescribed. The S-N approach can only quantify the
74 accumulated damage without providing any information about the size and dimensions of the
75 damage. Fracture mechanics on the other hand estimates time-dependent fatigue crack size. In
76 OWT structures, due to access restrictions, the choice of the NDT method can be limited to a
77 certain NDT method with a specific detection capability. Therefore, it may be necessary to
78 consider the Probability of Non-Detection (PoND) and improve the design for such a scenario.

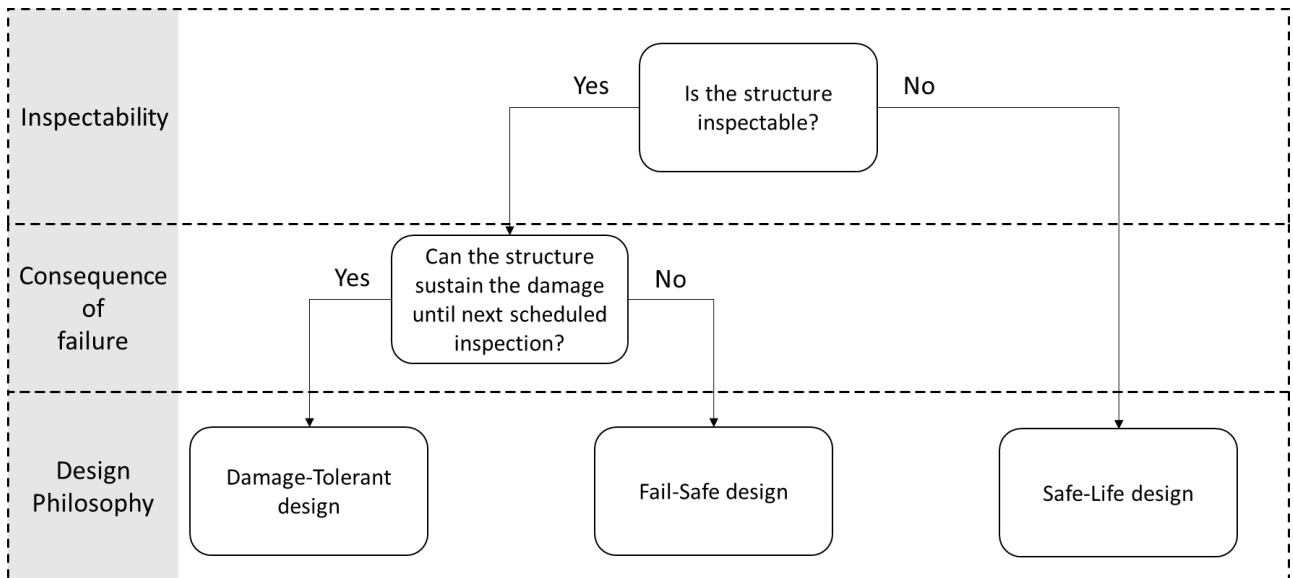


Figure 1 Relationship between inspection and fatigue design philosophy

Effect of larger defect sizes: S-N data is based on the assumption that the initial defect sizes are small, typically between 0.04 to 0.2 mm (BSI7608, 2015), assuming that an appropriate fabrication quality control program is in place which can detect larger fabrication defects. In practice, the reliability and efficiency of such a program and the NDT techniques are uncertain and vary considerably among fabrication yards (Amirafshari, 2019). Assessment and design of the welded joints considering the presence of large defects is only possible using a Fracture Mechanics approach. An improved joint design can be achieved allowing for possible fabrication defects by, for example, specifying larger thicknesses, higher toughness steels, post-weld heat treatment, etc (Zerbst et al., 2015).

New welding processes: There are always efforts to improve structural resistance, fabrication efficiency and weld quality by developing and implementing new welding technologies. Those processes may inevitably have altered characteristics (defect rates, sizes, and geometry, residual stresses, material toughness, etc.), which affect fatigue failure of the joint. Considering these variables using S-N data will require the development of a bespoke fatigue test program which is not always feasible (Lassen and Recho, 2013). A more efficient and cost-effective solution is the application of fracture mechanics.

New materials: development and use of new steel grades with higher tensile strength and weld consumable with superior weldability characteristics affect fatigue life. I.e. higher strength steel will be capable of resisting higher stresses, but the fatigue resistance does not increase proportionally (Okumoto et al., 2009). Contrary to the S-N method, these variables can be directly considered in the fatigue life prediction using Fracture Mechanics.

Shakedown, and compressive residual stresses: Fracture failure of welded joints is directly related to weld residual stresses. Tensile residual stress reduce fatigue life by reducing fracture capacity and moving the compressive part of cyclic stress to the tensile stress region. Part of these stresses can be relieved under service or fabrication loads, which is commonly known as the “shake-down” effect (Li et al., 2007). In pile foundations, on the other hand, since the structure is driven to the soil a considerable amount of compressive residual stresses are induced into the pile (Da Costa et al., 2001), which can potentially improve the fatigue and fracture performance. The effect of compressive residual stress and the shakedown phenomena and its interaction with various flaw sizes can be addressed using a fracture mechanics approach.

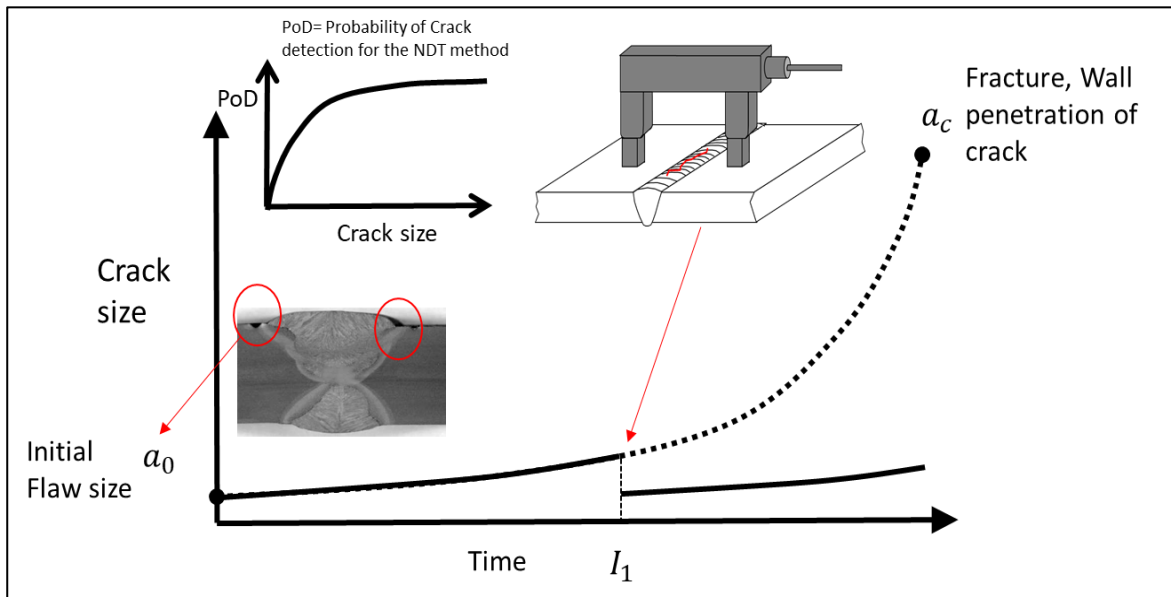
112 In this paper the fracture mechanics principals are briefly described, then a framework for an
 113 optimised design of structures based on fracture mechanics is developed. Then, probabilistic
 114 fracture mechanics for risk and reliability-based design approaches are outlined. Finally, the
 115 application of the developed methods to a Monopile support structure is demonstrated.

116 2 Fracture Mechanics Approach

117 Fatigue cracks in welded structures initiate from weld fabrication defects at the joints. Even
 118 sound welded joints often contain small undercuts (Figure 2).

119 The fracture mechanics approach uses the Paris equation to predict crack growth under cyclic
 120 stress. The method is based on the assumption that an initial flaw is present in the structure.
 121 The initial flaw size depends on the rigour of the fabrication quality control (QC) program
 122 (Jonsson et al., 2016). The reliability of the NDT method that is used during the QC, the extent
 123 of the inspection (100% or partial) and the flaw acceptance criteria will influence such a rigour.

124 The fracture mechanics enables the efficient application of NDT methods for in-service
 125 inspection by specifying inspection interval(s) and the most effective NDT which has the
 126 capability of reliable detection of the predicted crack size with required confidence. This is
 127 illustrated in Figure 2 below, where the NDT inspection (I_1) detects cracks greater than initial
 128 flaw size (a_0). If all such cracks are found and repaired the crack growth curve will be shifted
 129 down.



130
 131 **Figure 2 Crack growth curve diagram**

132 2.1 Crack growth prediction

133 Fracture mechanics (FM) enables the prediction of crack propagation by using the crack growth
 134 rate, illustrated in Figure 3. Region A is where the crack growth rate occurs as soon as $\Delta K \geq$
 135 ΔK_{th} , where ΔK_{th} is the threshold value of ΔK . The threshold value depends on a number of
 136 factors such as the stress ratio $= K_{max}/K_{min}$, sequence effect, residual stresses, loading
 137 frequency, and the environment. Region B is where the crack growth rate increases with ΔK to
 138 a constant power. Region C is where the crack growth rate increases rapidly until failure occurs
 139 as soon as $K \geq K_{critical}$.

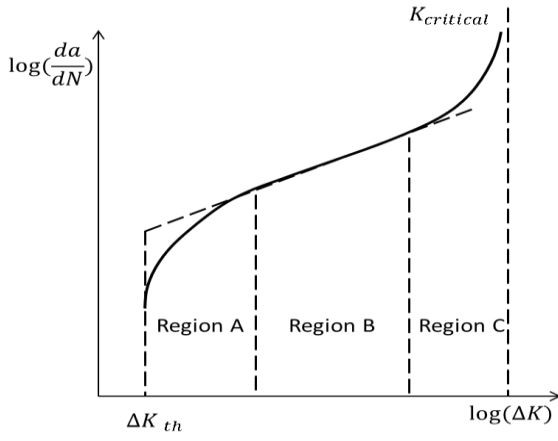


Figure 3 Schematic of crack propagation curve according to Paris-Erdogan law (Amirafshari, 2019)

In the FM approach crack growth rate is commonly described by the Paris-Erdogan Eq. (1):

$$\frac{da}{dN} = C * \Delta K^m \quad (1)$$

where, $\frac{da}{dN}$ is the rate of crack growth to load cycles, ΔK is the change in stress intensity factor, and C and m are material constants. Recently a bilinear crack growth model has been used, as well (Figure 4). BS7910:2015 (British Standard, 2019) recommended model is the bilinear model, while the simplified model is cited, as well.

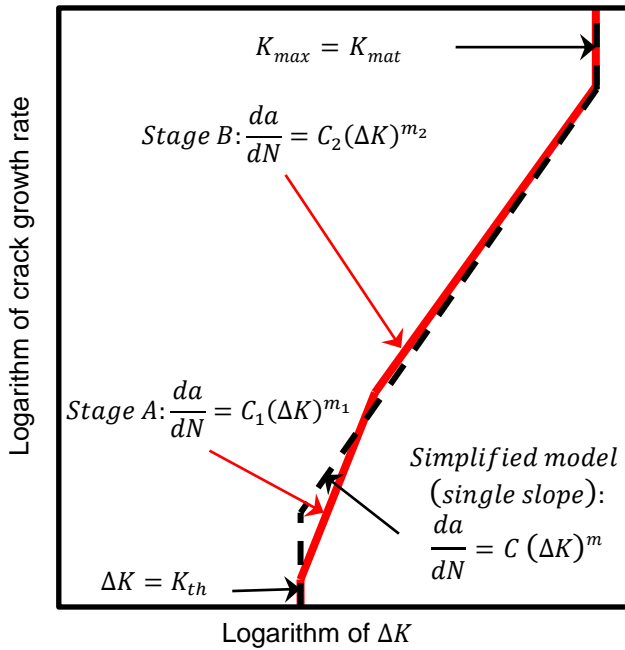


Figure 4 Schematic of crack growth models by Paris law

Stress intensity factor is described by:

$$\Delta K = Y\sigma\sqrt{\pi a} \quad (2)$$

where, a is flaw size, σ is stress at the flaw, and Y is the geometry function which depends on both the geometry under consideration and the loading mode. There are several ways in which solutions for Y can be obtained. Although it is possible to derive solutions for simple geometries

153 analytically, e.g. using ‘weight functions’, numerical techniques are more commonly used (finite
154 elements, finite difference or boundary elements methods).

155 The number of cycles to failure is calculated by rearranging and rewriting Eq. (1):

$$N = \int_{a_0}^{a_f} \frac{da}{C(\Delta K)^m} = \frac{1}{A * Y^m * \Delta \sigma^m * \pi^{\frac{m}{2}}} * \frac{a_f^{\left(1-\frac{m}{2}\right)} - a_0^{\left(1-\frac{m}{2}\right)}}{1 - \frac{m}{2}} \quad (3)$$

156 Offshore structures are not subjected to constant amplitude stress, but a variable amplitude
157 stress spectrum. If the long-term stress distribution is converted into a step function of n blocks
158 generally of equal length in $\log N$, the crack size increment for step i is:

$$\Delta a_i = C(\Delta K_i)^m \Delta N_i \quad (4)$$

159 moreover, the final crack size at the end of the N cycles is obtained by summing Eq. (4) for the
160 n stress blocks:

$$a_N = a_0 + \sum_{i=1}^N \Delta a_i \quad (5)$$

161 Equation (4) is only valid for small values of Δa_i since ΔK_i depends on the crack size, which
162 requires dividing the stress range spectrum into a large number of stress blocks.

163 The number of cycles to failure may, alternatively, be calculated according to Eq. (6) using an
164 equivalent constant amplitude stress ranges $\Delta \sigma_{eq}$ giving the same amount of damage (Naess,
165 1985):

$$\Delta \sigma_{eq} = \left[\int_0^\infty \Delta \sigma^\beta p_{\Delta \sigma}(\Delta \sigma) d\Delta \sigma \right]^{1/\beta} \quad (6)$$

166 where β is the contribution factor. For the central part of the crack growth curve β is often taken
167 as the slope of the of the crack growth line. $p_{\Delta \sigma}(\Delta \sigma)$ is the probability density function of stress
168 range $\Delta \sigma$.

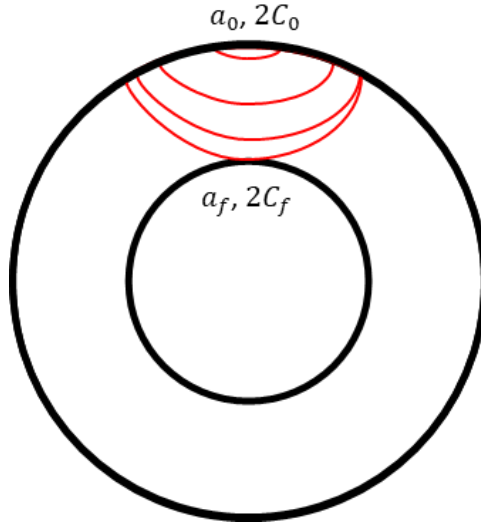
169 2.2 Failure criteria

170 2.2.1 Through thickness

171 In the through-thickness criterion, the initial fatigue crack is assumed to be a surface-breaking
172 flaw growing along the height (a) and length ($2C$) of the flaw. The failure happens when the
173 crack height penetrates through the thickness of the wall (Figure 5). This criterion is,
174 particularly, commonly adopted for structures containing pressurised containments e.g.

175 pipelines, pressure vessels, etc. or air-filled offshore structure, where the pressure or absence of
 176 water inside the structure can be used as a simple way to detect through-thickness cracks.

177



178 **Figure 5 Diagram of a surface crack penetrating the wall**

179 2.2.2 Total Collapse criteria

180 Many structures have the capacity to sustain through-thickness cracks until the crack length
 181 reaches a critical length. Thin wide plates that are primarily subjected to membrane stress and
 182 redundant structures such as jacket type platforms and stiffened plate hull structures are
 183 examples of such structures.

184 In structural reliability analysis, the probability of a collapse can be considered as a probability
 185 of a fatigue crack failure, P_F , times the probability of a collapse given that there is a fatigue
 186 failure in the structure, P_{SYS} . The probability of the total structural collapse due to fatigue failure
 187 should be below a target probability of failure, P_t :

$$P_F * P_{SYS} \leq P_t \quad (7)$$

188 For jacket structures, the method of removing one member has been commonly used to assess
 189 the residual capacity against overall collapse (DNV, 2015).

190 2.2.3 Critical crack size

191 Fatigue failure is considered to occur when the crack size reaches a critical value. There are
 192 generally two ways to determine the critical size, which is explained in the coming sections:

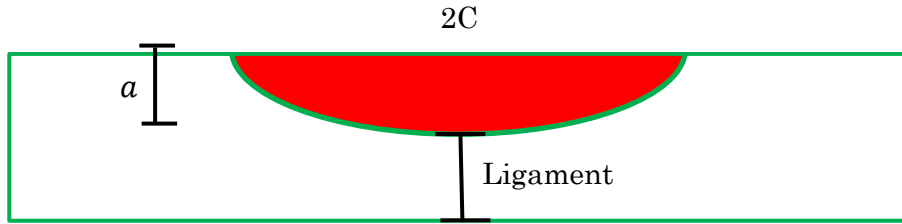
- 193 1. Based on the geometry of the structural member
- 194 2. Based on the Failure Assessment diagram

195 The critical size maybe then reduced to account for further safety factors.

196 2.2.3.1 Based on the geometry of the structural member

197 For ductile structures, it is common to take the material thickness as the critical crack height
 198 ($a_f = a_{cr} = Thickness$). However, normally the assumption is that the crack grows under cyclic
 199 loading which corresponds to normal service loading until it becomes through the thickness. In
 200 reality, failure often happens during extreme load occurrences. The cracked structure may fail
 201 under such extreme loading through the failure of the thickness ligament (Figure 6). The

202 brittle or elasto-plastic ligament failure may also occur in structures with low fracture
203 toughness.



205 Figure 6 Diagram of the remaining ligament in a semi-spherical crack

206 To address the above limitation the failure assessment diagram (FAD) may be adopted.

207 2.2.3.2 Based on the Failure Assessment Diagram (FAD)

208 Failure Assessment Diagram (FAD) can assess the failure of the through-thickness crack as
209 well as implementing extreme load occurrences by treating them as the primary stress. The
210 approach is explained below.

211 When a crack propagates through a structure, ultimately the crack size reaches a critical size
212 a_f . a_f corresponds to a critical stress intensity factor, usually taken as characteristic of the
213 fracture toughness K_{mat} , at which fracture happens. Alternatively, if the applied load is high
214 and the structure tensile strength is low, the structure may reach its tensile strength capacity
215 and fail by plastic collapse. The latter is more favourable as it is usually associated with large
216 deformations prior to failure providing some level of warning. In between brittle fracture and
217 global collapse is an elastoplastic failure mode, where failure occurs before reaching the plastic
218 capacity or toughness limit; this has been best described by failure assessment diagram (FAD)
219 in the R6 procedure in 1976 and improved over time by e.g. including the options available to
220 model specific material properties. The body of knowledge encapsulated in R6 affected the
221 development of British Standards documents in various ways over the years, leading to
222 BS7910:1999 and the latest version at the time of writing, (British Standard, 2019).

223 The failure assessment line (FAL) represents the normalised crack driving force:

$$K_r = \frac{K_{elastic}}{K_{elastic\ plastic}} \quad (8)$$

224 K_r is equal to 1 where the applied load is zero and declines as the ratio between the applied load
225 and yield load (L_r) increases towards collapse load (see Figure 7).

226 The plastic collapse load is calculated based on yield stress. However, the material has further
227 load carrying capacity as it work-hardens through yield to the ultimate tensile stress. To take
228 this into account the rightwards limit of the curve is fixed at the ratio of the flow stress to the
229 yield stress:

$$L_r = \frac{\sigma_{flow}}{\sigma_Y} \quad (9)$$

230 The flow stress is the average of the yield and ultimate stresses:

$$\sigma_{flow} = \frac{\sigma_Y + \sigma_U}{2} \quad (10)$$

If the assessment point lies inside the envelope (below the FAL), the fracture mechanics driving parameter is lower than the materials resistance parameter and the part should be safe, otherwise, there is a risk of failure. The failure assessment diagram can be determined with one of the procedures provided by (British Standard, 2019). As it is illustrated in Figure 7, FAD may be categorised into three different zones: Zone 1 is the fracture dominant zone, Zone 2 is the elastoplastic region or the knee region, and Zone three is the collapse dominant zone.

(British Standard, 2019) has three alternative approaches Option 1, Option 2 and Option 3. These are of increasing complexity in terms of the required material and stress analysis data but provide results of increasing accuracy.

Options 1&2 (British Standard, 2019) and Option 2A/3A (British Standard, 2019) for structural steel with Ultimate tensile stress of 550 MPa and Yield stress of 450 MPa are illustrated in Figure 7. It can be seen that the greatest difference between the three plotted locus is in the collapse region. For discussions about BS7910 options, reference is made to (British Standard, 2019; TWI, 2015).

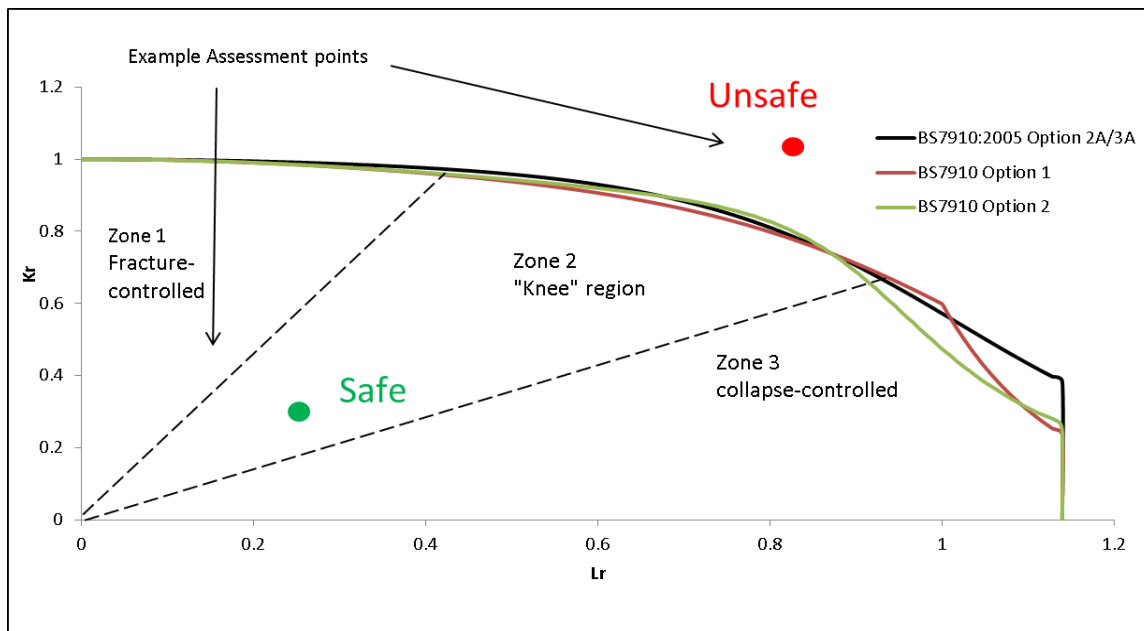


Figure 7 Failure Assessment Diagram (FAD) (Amirafshari, 2019)

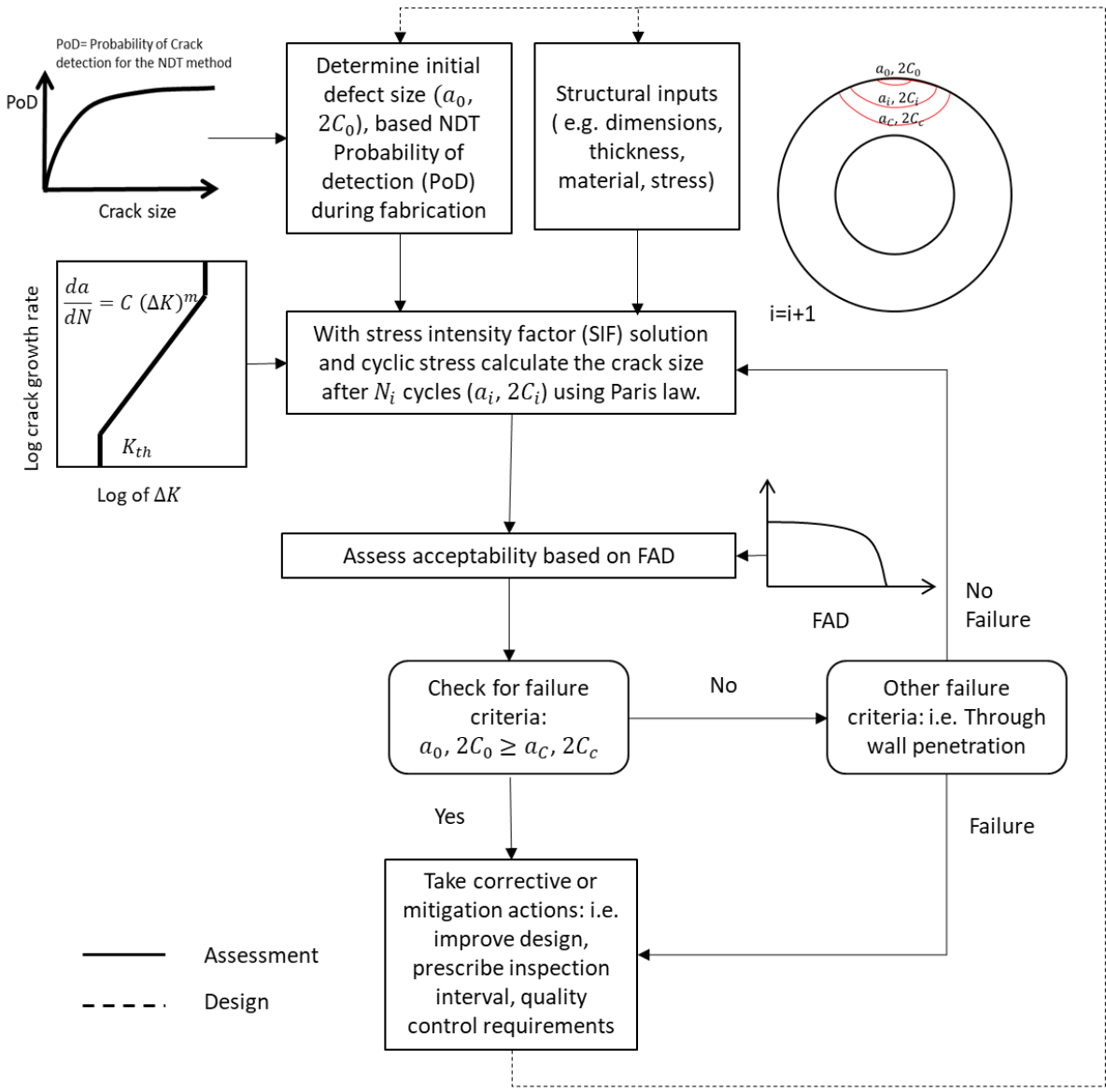
3 Fracture Mechanics framework for structural design

The common practice in structural design is to specify dimensions of the structural component based on the most critical limit state, usually ultimate limit state (ULS), and check or modify the design based on other limit states such as serviceability limit state (SLS) or fatigue limit state (FLS).

In OWT support structures fatigue failure initiates from the welded connection, thus, the fatigue design often involves prescribing local improvements to the welded connection. However, since fatigue life is related to dynamic characteristics of the structure the global dimensions of the structure may also need alterations to achieve higher fatigue resistance.

256 The fatigue damage prediction model could be the S-N curve method or the Linear Elastic
 257 Fracture Mechanics (LEFM). Here, a LEFM method is adopted to address the limitations of the
 258 S-N curve method. Figure 8 shows the proposed framework.

259 First, the required inputs, such as structural dimensions (determined by structural design
 260 based on ULS), initial flaw size, material toughness and tensile properties, stress at the flaw,
 261 and parameters of the Paris equation, are determined, using the Paris equation for a chosen
 262 increment of time (N_i), the increase in initial crack size is estimated. The predicted crack size is
 263 then compared against failure criteria. The procedure is repeated for the next time increment
 264 until the failure. If the failure is predicted to occur before the intended life of the structure the
 265 fatigue life may be enhanced by changing variables that affect the fatigue failure such as
 266 structural dimensions, quality control requirements (initial flaw size), post-fabrication
 267 improvements (e.g. post-weld heat treatment), or by specifying inspection interval(s).



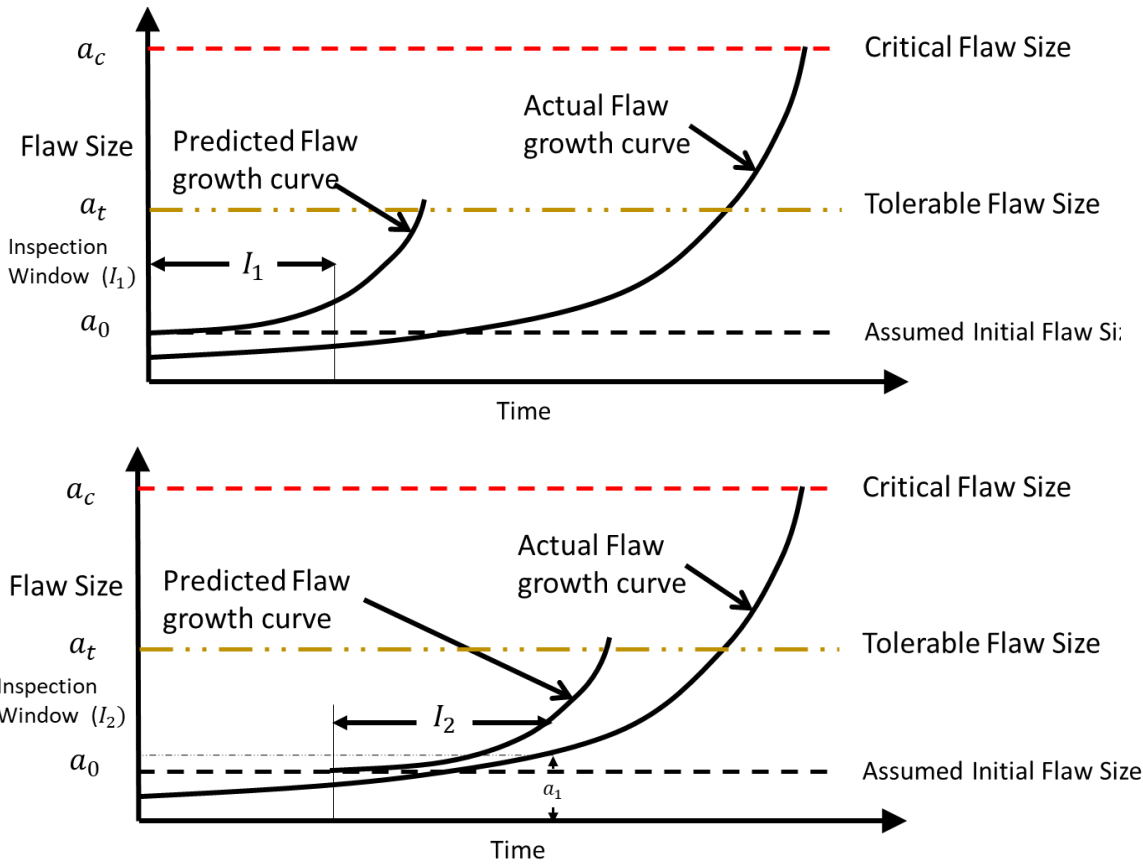
268
 269 **Figure 8 Fracture Mechanics flow diagram for assessment and design of structures against fatigue failure**

270 **3.1 Damage-tolerant design**

271 The term damage-tolerance fracture mechanics normally refers to a design methodology in
 272 which fracture mechanics analyses predict remaining life, and specifies inspection intervals.
 273 This approach is typically applied to structures prone to time dependent crack growth. The

274 damage tolerance philosophy allows flaws to remain in the structure, provided they are well
 275 below the critical size.

276 Once the critical crack size, a_c , has been estimated, a safety factor is applied to determine the
 277 tolerable flaw size a_t . The safety factor should be based on uncertainties in the input parameters
 278 (e.g. stress, parameters in the Paris equation and toughness). Another consideration in
 279 specifying the tolerable flaw size is the crack growth rate; a_t should be chosen such that da/dt
 280 at this flaw size is relatively small, and a reasonable length of time is required to grow the flaw
 281 from a_t to a_c (Anderson, 2005). This is shown schematically in Figure 9.



282
 283 **Figure 9 schematic representation of damage tolerant fracture mechanics approach, adapted from** (Anderson, 2005)

284 **3.2 Inspection reliability**

285 NDT techniques can only detect a limited number of defects of a certain size. For instance, an
 286 NDT method with 50% probability of detection at a certain size, is expected to miss 50% of the
 287 defects of that size, in other words, the real number of the defects with that size is likely to be
 288 100% more than the detected. In structural integrity assessment, it is often convenient to plot
 289 detection probability against defect size, which constructs the so-called probability of detection
 290 curve (Figure 11). Detection capabilities of NDT methods are directly related to the sizing of
 291 flaws (Georgiou, 2006). The bigger the flaw sizes, the more likely that they are detected. Figure
 292 10 shows the relationship between detected defect size distribution, the probability of detection
 293 of defect sizes and the actual defect size distribution that are present in the structure.

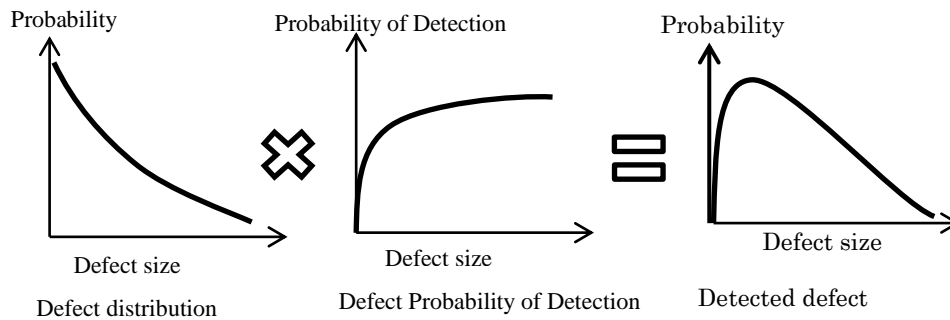


Figure 10 Relationship between crack size distribution, Probability of detection and detected crack size distribution (Amirafshari, 2019)

Probability of Detections PoDs for NDT methods are highly dependent on various factors such as the operator skills, testing environment, test specimen (thickness, geometry, material, etc.), type of the flaw, orientation and location of the flaw (Førli, 1999). Hence, an accurate estimation of PoD curves requires individual PoD test programs for specific projects. However, a number of lower bound generic models are available in the literature for some specific NDT methods. Two of such models, that are relevant to this work, are given in Figure 11 and Table 1 below.

Further information about derivation, application and limitations of PoD can found in (Georgiou, 2006).

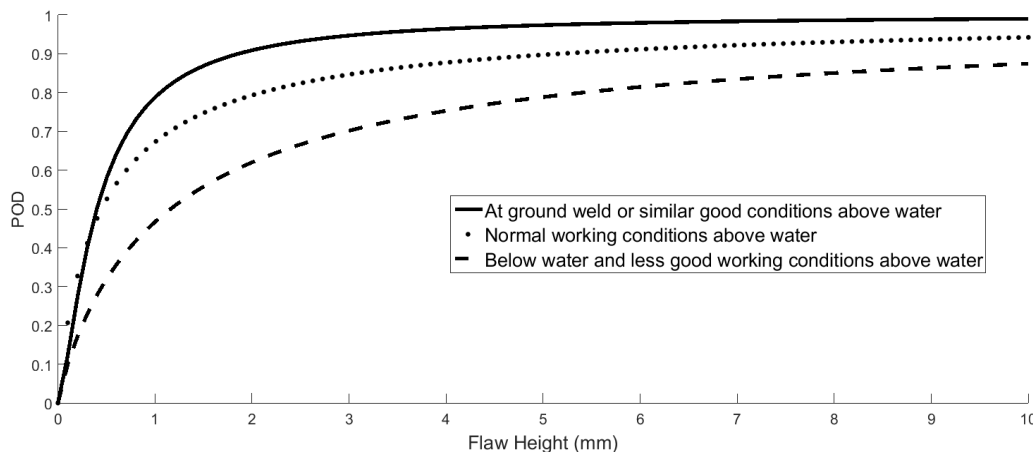


Figure 11 DNV PoD for surface NDE. Replotted from (DNV, 2015)

Method	Condition		Flaw Length mm	Flaw through-thickness mm
Magnetic Particle Inspection (MPI)	Machined or ground		5	1.5
	As-welded	With local dressing	10	2
		With poor profile	20	4
Ultrasonic Testing (UT)	Convictional		15	3

Table 1 NDT Reliability (BS7910, 2015)

3.3 Inspection strategy

Fracture mechanics assessment is closely tied to the inspection method. The inspection method provides input to the fracture mechanics assessment, which in turn helps to define inspection intervals. A structure is inspected during construction for quality control purposes. Choice of the NDT method varies between fabrication yards, but as a general rule, all weldments are visually inspected and may be complemented by inspection of a limited number of checkpoints

314 using more reliable NDT techniques on a sampling basis (Amirafshari et al., 2018). If no
 315 significant flaws are detected, the initial flaw size is set at an assumed value a_0 , which
 316 corresponds to the largest flaw that might be missed by NDT.

317 Generally, there are two strategies in the inspection of structures that are susceptible to damage
 318 mechanisms:

319 3.3.1 The inspection schedules are fixed (Periodic Maintenance):
 320 Here, the fracture mechanics can be used to design the structure so that the possible fatigue
 321 cracks remain below tolerable limits. The crack size at the time of the inspection is predicted
 322 using the Paris law to select an appropriate NDT method.

323 3.3.2 Inspection schedule is not fixed (Condition Based Maintenance):
 324 In this case, the inspection interval and the NDT method can be optimised in such a way that
 325 the inspection results in a safer condition or a minimised cost of maintenance and failure.

326 3.4 Design inputs
 327 Design inputs can be categorised into design constraint(Table 2) and design variables (Table 3).
 328 Here, only design variables related to a fracture mechanics method are considered. Further
 329 information about the design of offshore wind turbine support structures can be found in (Arany
 330 et al., 2017) and (Van Wingerde et al., 2006).

331 Depending on the chosen maintenance strategy the inspection capabilities may be considered
 332 as design constraint or design variable.

333 If a probabilistic approach is employed instead of the conventional deterministic approach, the
 334 variables are considered stochastically and target probabilities of failures are used instead of
 335 allowable deterministic values (Table 2).

Design Constraint		
Limit State	Deterministic	Allowable damage, stress, etc.
	Probabilistic	Target levels of reliability
Inspection capabilities	During fabrication	<ul style="list-style-type: none"> Extend of inspection NDT PoD
	During service	<ul style="list-style-type: none"> Inspection schedule (fixed periodic inspections) NDT method (e.g. PoD, access restrictions, costs)

336 Table 2 Design constraints for damage tolerant fracture mechanics design

Design variables	Inspection and Monitoring options (Condition Based Maintenance)	NDT methods
		Condition monitoring
	Design options	Structural design options: <ul style="list-style-type: none"> Thickness Redundancy Material selection
		Fabrication specifications: <ul style="list-style-type: none"> Weld profile improvements Post Weld Heat Treatment Quality Control(i.e. NDT during fabrication, Tolerance limits)

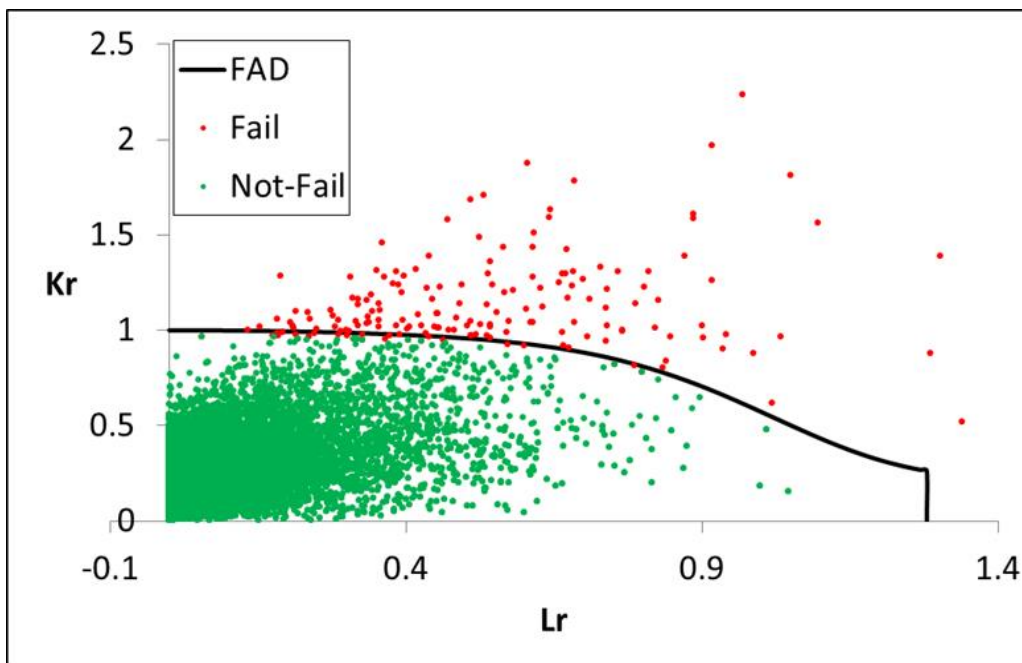
337 Table 3 Design variables for damage tolerant fracture mechanics design

338 4 Probabilistic Fracture Mechanics

339 Fracture mechanics approaches are commonly used deterministically and generally have a
340 hierarchical nature, i.e. the analyst may progressively reduce the level of conservatism in
341 assumptions by increasing the complexity level of the analysis and consequently the precision
342 of results until the operation of the structure is found to be fit-for-service. Otherwise, the
343 structure will require a repair, a reduction of service (for example lowering primary stress) or
344 resistance improvements (i.e. reduction of secondary stresses by stress relief techniques). This
345 type of approach is particularly useful in the assessment of safety cases where the aim is to
346 demonstrate that the structure is safe.

347 In deterministic analyses, uncertainty in variables is dealt with by taking upper bound and
348 lower bound of those variables- upper bound values of applied variables such as stress and flaw
349 size, with lower bound values of resistance variables such as fracture toughness. In reality, the
350 probability of all unfavourable conditions occurring at the same time is very low and often too
351 conservative. An alternative approach is a probabilistic analysis, in which, uncertain variables
352 are treated stochastically and as random variables.

353 In probabilistic assessments, all possible combinations of input variables leading to failure are
354 compared against total possible combinations, and a probability of failure is estimated instead
355 of a definite fail or not-fail evaluation. Probabilistic analysis is also in-line with the damage
356 tolerant philosophy. The failure probability for the limit state function may be estimated using
357 one of the available analytical, numerical or simulation methods such as the Monte Carlo
358 simulation. Figure 12 shows a Probabilistic fracture assessment using the Monte Carlo method
359 and based on the FAD.



360
361 **Figure 12 Probabilistic fracture assessment using the Monte Carlo method and based on FAD (Amirafshari, 2019)**

362 One limitation of deterministic fracture mechanics is that conservative prediction of critical
363 defect size and the time to the failure may reduce inspection efficiency by targeting wrong defect
364 sizes and at a wrong time in service, whereas probabilistic assessment will provide a more
365 efficient result (Lotsberg et al., 2016). Probabilistic failure assessment of the structures is also
366 known as Reliability analysis. These two terminologies are often used interchangeably.

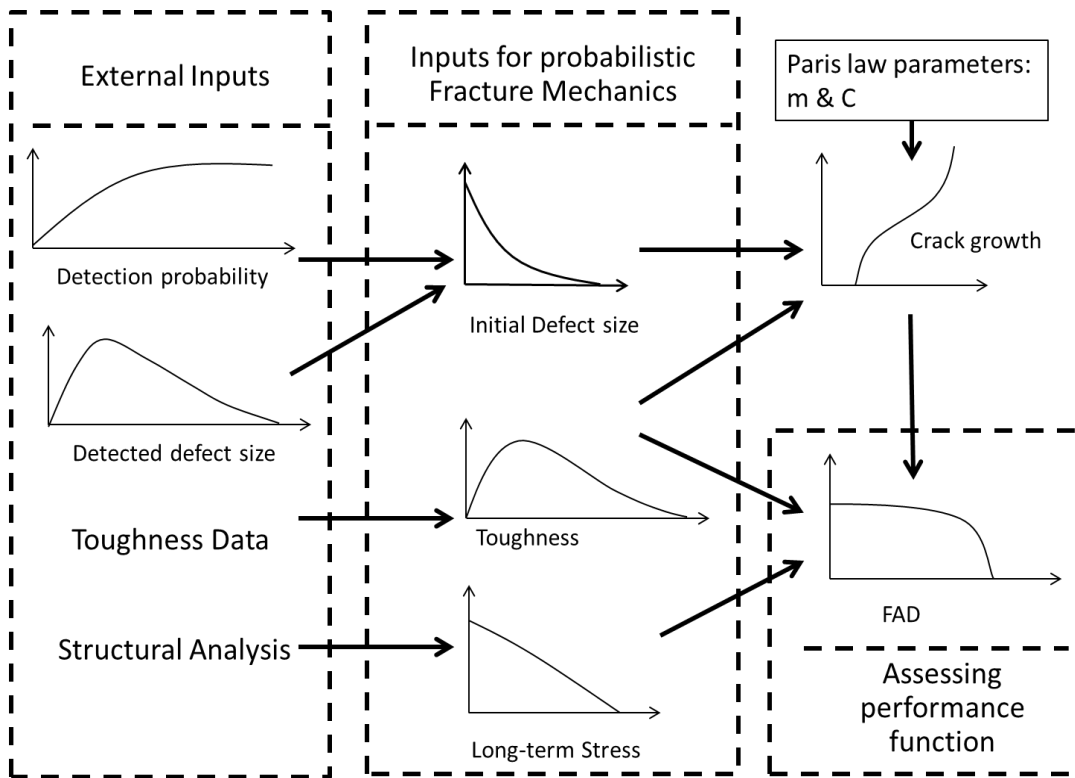


Figure 13 A schematic presentation of the inputs to Probabilistic Fracture Mechanics (Amirafshari, 2019)

Figure 13 shows the schematic presentation of the inputs to probabilistic fracture mechanics. Probabilistic fatigue and fracture analysis will predict the time-dependent failure probability of the structure (Figure 14). The predicted reliability will then need to be compared against an appropriate target reliability level.

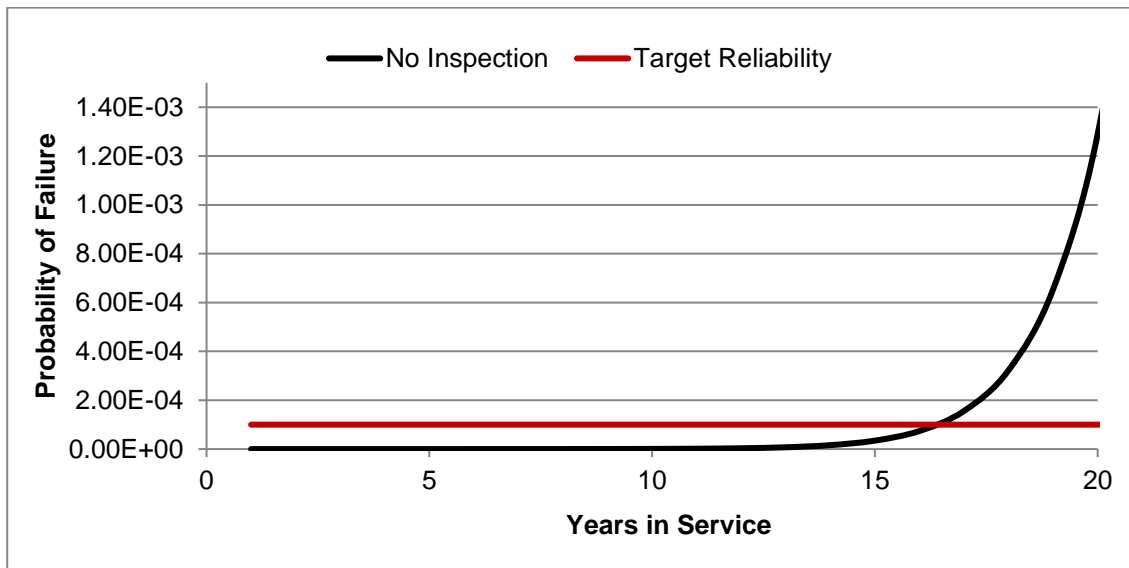


Figure 14 Example of a time-dependent fatigue and fracture reliability curve

4.1 Target reliability levels

Target reliability values may be employed to ensure that a required level of safety is achieved. The target reliability measures depend on the failure consequence as well as the cost and effort to reduce the risk of failure. The consequence of failure can be the risk of human injury and fatality, economic consequence, and social impacts. The target reliability should always correspond to a reference period, e.g. annual or service life probability of failure. If the relevant

consequence is the risk of human life, annual failure probabilities are preferred to ensure a consistent level of tolerable risks at any time. Target reliabilities may be defined in four different ways:

1. The standard developers recommend a reasonable value. This method is used for novel structures.
2. Reliability implied by standards. The level of risk is estimated for a design standard that is considered to be satisfactory. This method has been commonly used for standard revisions, particularly where the intention has been to provide a more uniform safety level for different structural types and loading types. By carrying out a reliability analysis of the structure satisfying a specific code using a given probabilistic model, the implicit required level in this code will be obtained, which may be applied as the target reliability level. The advantage with this approach compared to applying a predefined reliability level is that the same probabilistic approach is applied in the definition of the inherent reliability of the code specified structure and the considered structure, reducing the influence of the applied uncertainty modelling in the determination of the target reliability level.
3. The target level for risk assessment based on failure experiences. This method is particularly useful when the functional reliability of the system is more important than the reliability of individual components. In the automotive industry or electronic components manufacturing component reliability is determined by failure rate data of real components. The failure rate data is then used in system reliability calculation(Bertsche, 2008).
4. Economic value analysis (cost-benefit analysis). Target reliabilities are chosen to minimise total expected costs over the service life of the structure. In theory, this would be the preferred method, but it is often impractical because of the data requirements for the model.

Examples of target reliabilities prescribed by codes and standards are listed in Table 4. For further information about available models for developing target reliability levels for novel structures reference is made to (Bhattacharya et al., 2001).

	Scope	Limit state function	Minimum Reliability index	Maximum Probability of failure
Euro code. Basis of structural design (BSI, 2005)	buildings and civil engineering works	Ultimate limit states (ULS)	3.3 to 4.3 for 50 years reference period and 4.2 to 5.2 for annual	4.83×10^{-4} to 8.54×10^{-6} for 50 years reference period and 1.33×10^{-5} to 9.96×10^{-8} for annual
	Residential and office buildings, public buildings where consequences of failure are medium (e.g. an office building)	Fatigue limit state (FLS)	1.5 to 3.8 for 50 years reference period	6.68×10^{-2} to 7.23×10^{-5} for 50 years reference period
DNV (DNV, 1992)	Marine structures		3.09 to 4.75	1.00×10^{-3} to 1.02×10^{-6}

IEC61400-1	Offshore Wind Turbines	ULS & FLS	3.3	5.00×10^{-4}
DNV_OS_J101	Offshore Wind Turbines (unmanned structures)	ULS		1.00×10^{-4}
DNV_OS_J101	Offshore Wind Turbines (manned structures)	ULS		1.00×10^{-5}

Table 4 Examples of target levels of reliabilities specified by standards

4.2 Risk-Based design

The purpose of risk analysis is to comprehend the nature of risk and its characteristics including, where appropriate, the level of risk. Risk analysis involves a detailed consideration of uncertainties, risk sources, consequences, likelihood, events, scenarios, controls and their effectiveness. An event can have multiple causes and consequences and can affect multiple objectives (ISO-31000, 2018). The risk remaining after protective measures are taken is called residual risk (ISO-14971, 2012). The purpose of risk evaluation is to support decisions. Risk evaluation involves comparing the results of the risk analysis with the established risk criteria to determine where additional action is required (ISO-31000, 2018). The overall procedure for risk analysis and risk evaluation is a risk assessment (ISO-31000, 2018).

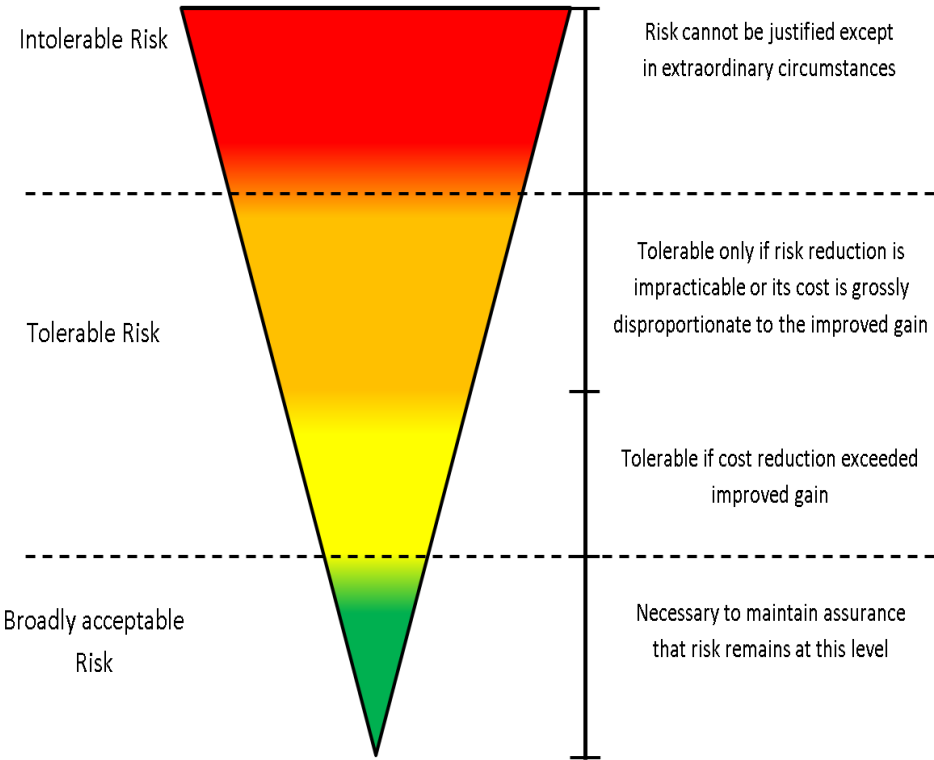
A commonly used method of risk evaluation is the so-called Risk Matrix model in which the failure probability is shown in one axis and the consequence of failure on the other. The failure probability and consequence failure may be specified quantitatively, qualitatively, or semi-quantitatively, depending on the complexity of the model and the availability of data. Each combination of failure probability and consequence of failure will then be assigned a corresponding risk level. It is useful to show these levels in specific colour coding convention. One such convention is an adapted traffic light convention in which low-risk levels are shown in green, extreme risks in red and medium risk levels are coloured in yellow. It is also possible to refine this colour coding further, for example, light yellow and dark yellow, to allow for more risk levels. An example Risk Matrix is shown in Figure 15.

Probability of failure	5. Frequent	HIGH	HIGH	EXTREME	EXTREME	EXTREME
	4. Likely	MEDIUM	HIGH	HIGH	EXTREME	EXTREME
	3. Possible	MEDIUM	MEDIUM	HIGH	HIGH	EXTREME
	2. Unlikely	LOW	MEDIUM	MEDIUM	HIGH	HIGH
	1. Rare	LOW	LOW	MEDIUM	HIGH	HIGH
		1. Negligible	2. Minor	3. Moderate	4. Major	5. Catastrophic
		Consequence of failure				

Figure 15 A typical Risk matrix diagram

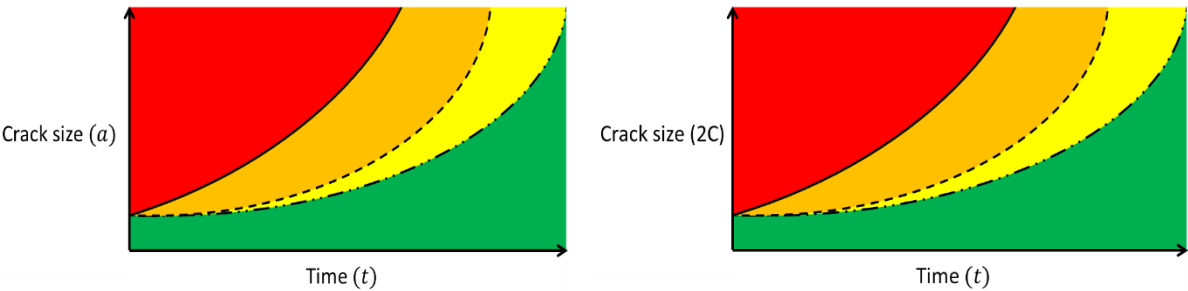
To assign an appropriate risk level (i.e. colour in the risk matrix) it is necessary to establish risk acceptance levels. If a system has a risk value above the accepted levels, actions should be taken to improve safety through risk reduction measures. One challenge in this practice is defining acceptable safety levels for activities, industries, structures, etc. Since the acceptance of risk depends upon society perceptions, the acceptance criteria do not depend on the risk value alone (Ayyub et al., 2002).

435 Another common risk evaluation method is the ALARP, which stands for "as low as reasonably
 436 practicable", or ALARA (as low as reasonably achievable) (HSE, 2001). The ALARP basis is that
 437 tolerable residual risk is reduced as far as reasonably practicable. For a risk to be ALARP, the
 438 cost in reducing the risk further would be grossly disproportionate to the benefit gained. The
 439 basis of ALARP is illustrated by the so-called carrot diagram in Figure 16.



440
 441 **Figure 16 ALARP Carrot diagram based on (HSE, 2001)**

442 By adopting a risk-based approach in fracture mechanics for a chosen design parameter the
 443 structural design may be assessed against the corresponding risk. As an example, the design
 444 stress levels for a particular initial crack size will be associated with the corresponding risk
 445 levels, as schematised in Figure 17.



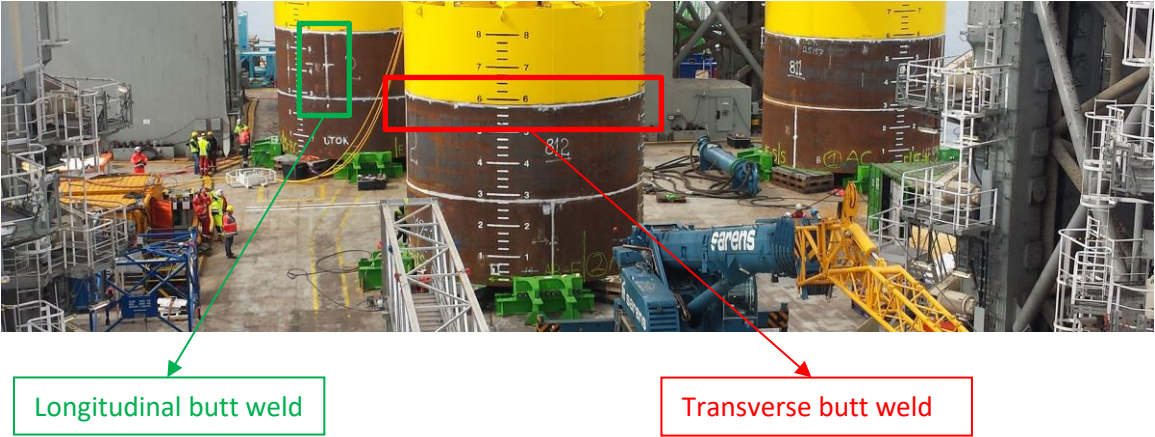
446
 447 **Figure 17 schematics of Crack growth curves based risk profile**

448 **5 Case-Study 1: Monopile OWT support structure**

449 Fatigue design based on a baseline NREL 5MW offshore wind turbine (OWT) supported on a
 450 monopile structure (Figure 19) is presented here. The framework illustrated in Figure 8 is used
 451 to conduct the fracture mechanics assessment. Table 5 summarises the inputs parameters used
 452 in this study. Further information about the structure and the Finite Element Analysis can be
 453 found in (Gentils et al., 2017).

454 Transverse butt weld (weld line perpendicular to the normal stress) are more prone to fatigue
 455 damage than the longitudinal butt joints (weld line parallel to the normal stress). Figure 18
 456 shows these joints in a monopile structure. A fatigue crack growing at the transverse butt weld
 457 toe located in the mud-line (Figure 19) is considered the most critical location.

458



459
 460

Figure 18 Monopile welded connections (twd, 2019)

Case Description		
Structure	NREL 5MW OWT	
Material Properties	Young Modulus	210 MPa (Gentils et al., 2017)
	Poisson Ratio	0.38 (Gentils et al., 2017)
	Yield stress (σ_Y)	355 MPa (Gentils et al., 2017)
	Tensile strength	550 MPa (Gentils et al., 2017)
	Toughness	200 MPa* m ^{0.5} assumed
Fatigue assumptions	Crack growth model	Single slope Crack growth
	Cyclic stress	Equivalent constant amplitude stress 51.2 MPa
	Stress Intensity Solution	A surface flaw in a Plate
	Paris Law Constants	$m = 3.9$, $C = 3.814 * 10^{-16}$ for Crack growing in HAZ and in Air, $m = 3.3$, $C = 4.387 * 10^{-14}$ for Crack in HAZ and in with free corrosion, (for da/dN in mm/cycle, and ΔK , in $N/mm^{0.5}$), (Mehmanparast et al., 2017)
	Design cycles in life	$N_{life} = \eta_a * \eta_{rated} * (20 [year] * 365[day per year] * [hour per year] * 60 [min per hour])$, for this structure = $1.253 * 10^8$ (Gentils et al., 2017)
Fracture assumptions	FAD	BS 7910 Option 1
	Primary stress	209 MPa (Gentils et al., 2017)
	Secondary stress	Weld Residual stress= 100 MPa, assumed
	Thickness (B)	60 (mm) (Gentils et al., 2017)
	Initial Flaw dimensions (a*2C)	(1.5 mm * 5 mm)

461 Table 5 Inputs for Fatigue and fracture mechanics assessment

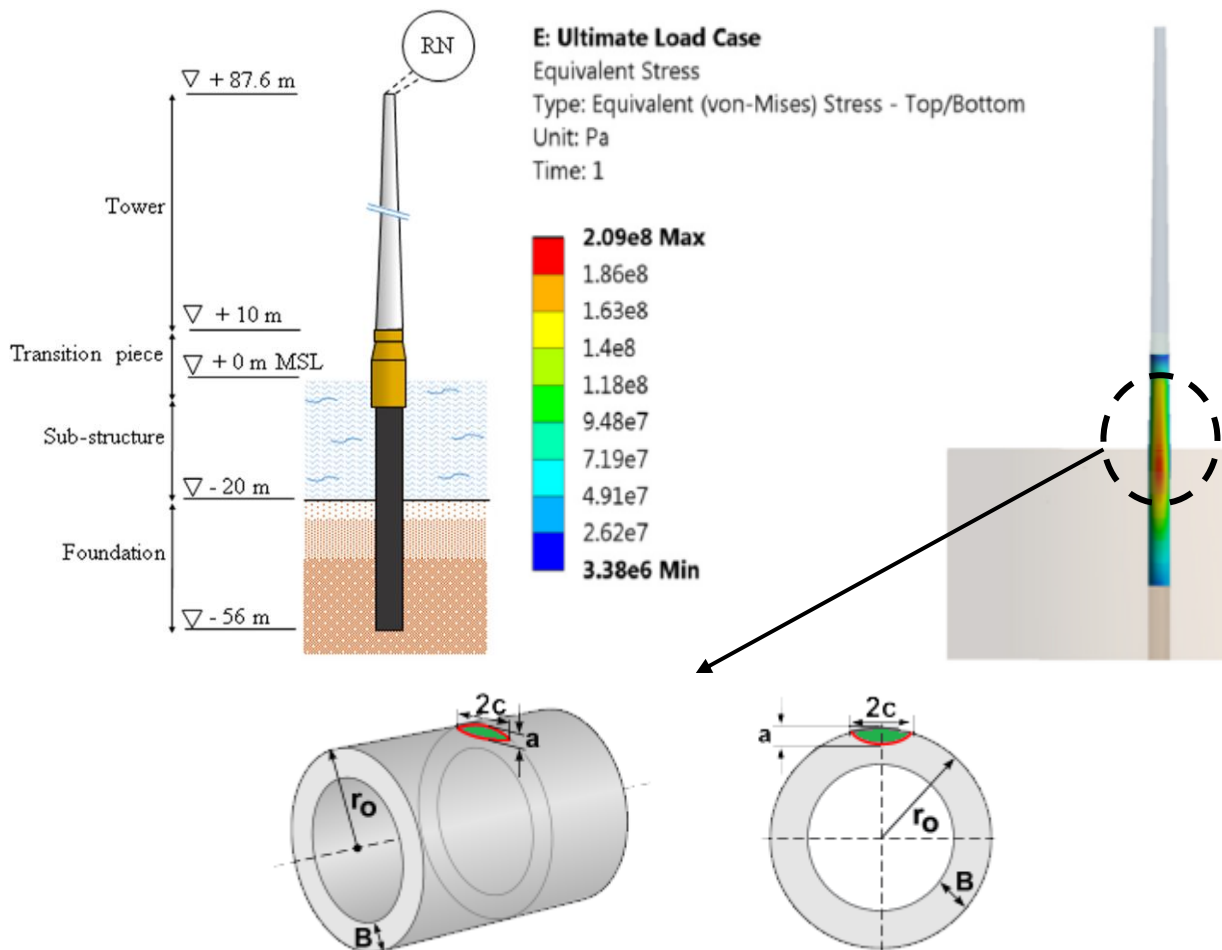


Figure 19 The case study structure diagrams and FEA contour plots for the support structure

Fatigue cracks normally initiate from small toe undercut weld defects (Figure 2), thus, in this study, a semi-spherical flaw growing in the heat-affected zone (HAZ) of the joint is considered. NDT inspection techniques are used during fabrication as part of the quality control scheme. MPI and UT are effective and commonly used method to detect surface breaking and embedded flaws, respectively. Here, the initial flaw size is conservatively assumed to be equal to 90 % PoD the NDT methods (Table 1). The primary fracture stress is taken as caused by ultimate limit state (ULS) design stress (Figure 19) corresponding to the parked wind turbine, under the 50-years Extreme Wind Model (EWM) with the 50-years Reduced Wave Height (RWH) and Extreme Current Model (ECM), defined as the Design Load Case (DLC) 6.1b and 2.1 for (IEC, 2019) and (DNV, 2013) standards, respectively. The crack growth stress is taken as the fatigue load case corresponds to an operating state under Normal Turbulence Model (NTM) and Normal Sea State (NSS) where wave height and cross zero periods are obtained from the joint probability function of the site, assuming no current; it corresponds to the DLC 1.2 from the IEC standard (IEC, 2019) and is assumed to represent the entire fatigue state (Gentils et al., 2017). Paris law parameters reported by (Mehmanparast et al., 2017) for offshore wind monopile weldments has been adopted. Other key assumptions and inputs for fatigue and fracture mechanics assessment are given in Table 5.

5.1 Crack growth in Air Environment

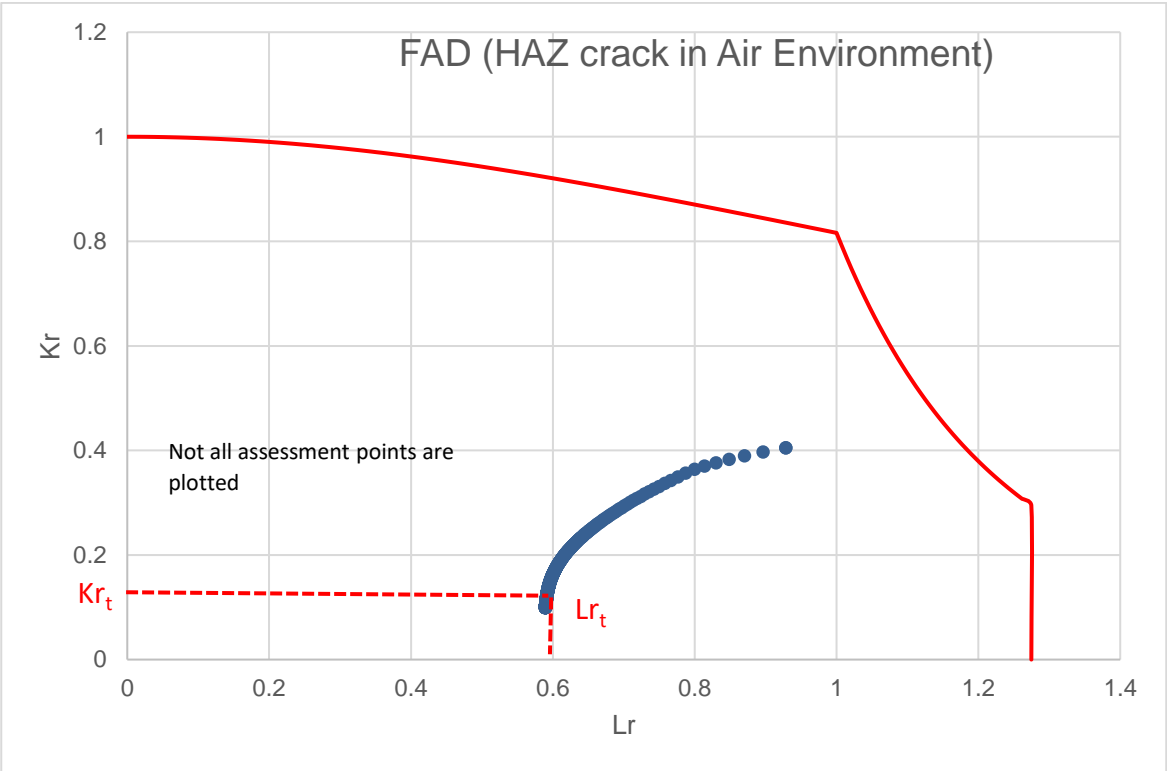
Crack growth parameters in the Paris equation for ferritic steels depend on the cyclic stress ratio, and environmental condition (Amirafshari and Stacey, 2019). In presence of effective corrosion protection measures, in-air conditions apply (British Standard, 2019).

485 Fatigue and fracture assessment results for cracks propagation in the air environment are given
486 in Table 6. In a tolerant design, the tolerable crack sizes need to be selected way below critical
487 sizes by considering some level of safety factors (Anderson, 2005). As described earlier, the
488 chosen tolerable crack size needs to be determined in a region of the crack size where crack
489 growth rate with respect to time is small to allow for a long time before failure but large enough
490 to be detected by the in-service inspection technique. Here, a tolerable crack height of 5.2 mm
491 is chosen which, depending on the inspection condition (Figure 11), gives 70 to 90 percent
492 Probability PoD. As shown in Figure 20, this will provide a good margin of safety and at least 6
493 years before failure (Figure 21).

Assessment results		
Critical Crack size	$a_c = 45 \text{ mm}$	$2C_c = 116 \text{ mm}$
Tolerable crack size (Assumed)	$a_t = 5.2 \text{ mm}$	$2C_t = 12 \text{ mm}$
	$Lr_t=0.592$	$Kr_t=0.128$

494 Table 6 results for crack growth in HAZ and in Air environment

495 Figure 20 shows assessment points from initial crack propagation at start of service life to the
496 final year of service. If the service continues beyond the design life (20 years), the structure is
497 likely to fail in elasto-plastic mode, providing reasonable level of plasticity from safety point of
498 view.



499 Figure 20 Failure assessment diagram (FAD) for crack growth in HAZ and in Air environment without inspection
500

501 As explained earlier a damaged tolerant design is closely tied to in-service inspection. Here, it
502 is assumed that an MPI inspection is carried out at year 12. When no crack is detected or
503 repaired if detected, the predicted crack size is updated and reduced back to the initial crack
504 size. This is shown with solid lines after year 12 in Figure 21. The final year crack size remains
505 below the tolerable limits.

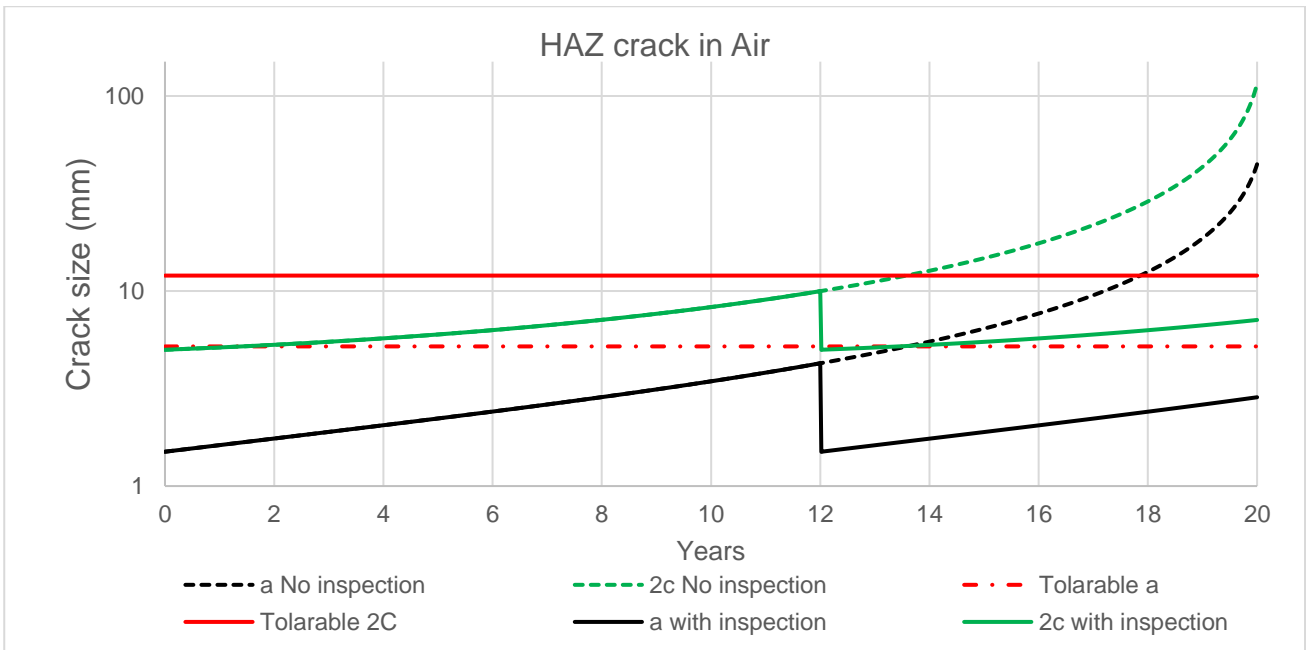


Figure 21 Crack growth curves for propagation in HAZ and in the Air environment

The weld profile condition may be as-welded or ground flushed depending on fabrication specification and could be altered by the design engineer. The effect of such condition was studied by considering the influence of weld profile on PoD for the MPI method. MPI can find smaller cracks in the welds with ground flushed crowns (Table 1). As shown in Figure 22 improving the weld joint design by specifying ground flushing requirement reduces the inspection frequency from twice to once in 20 years of service.

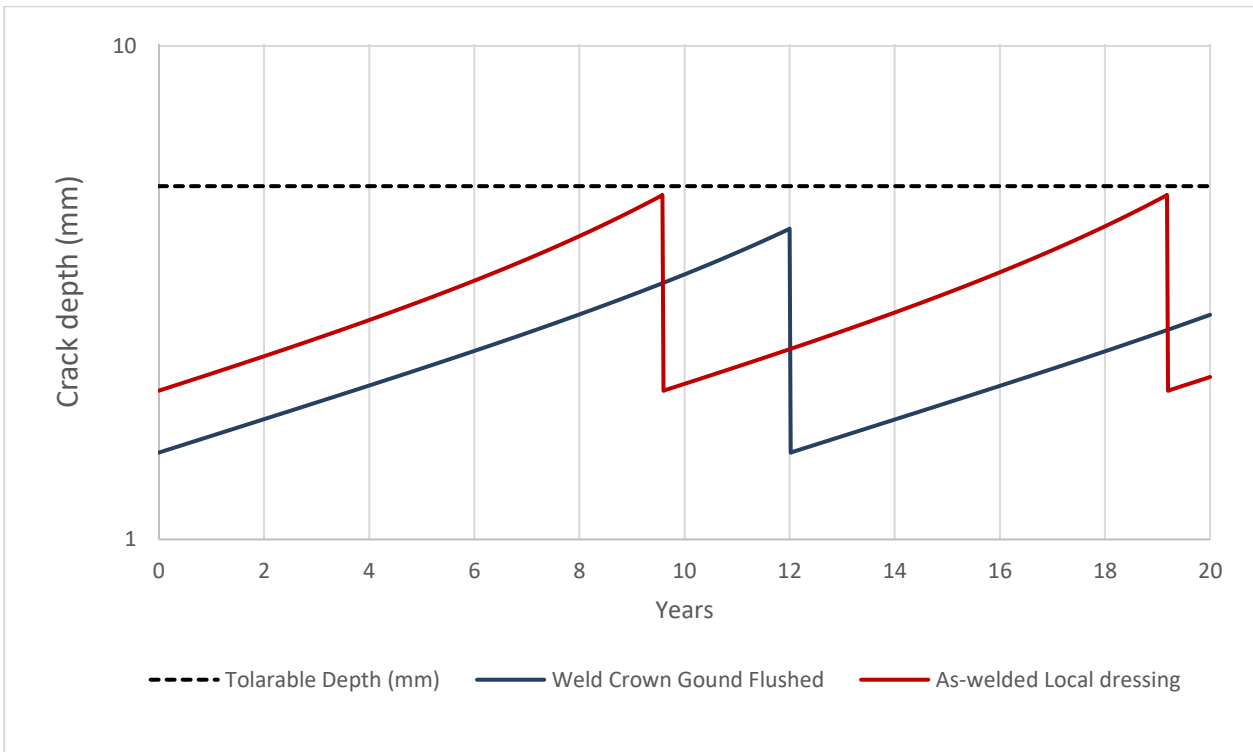
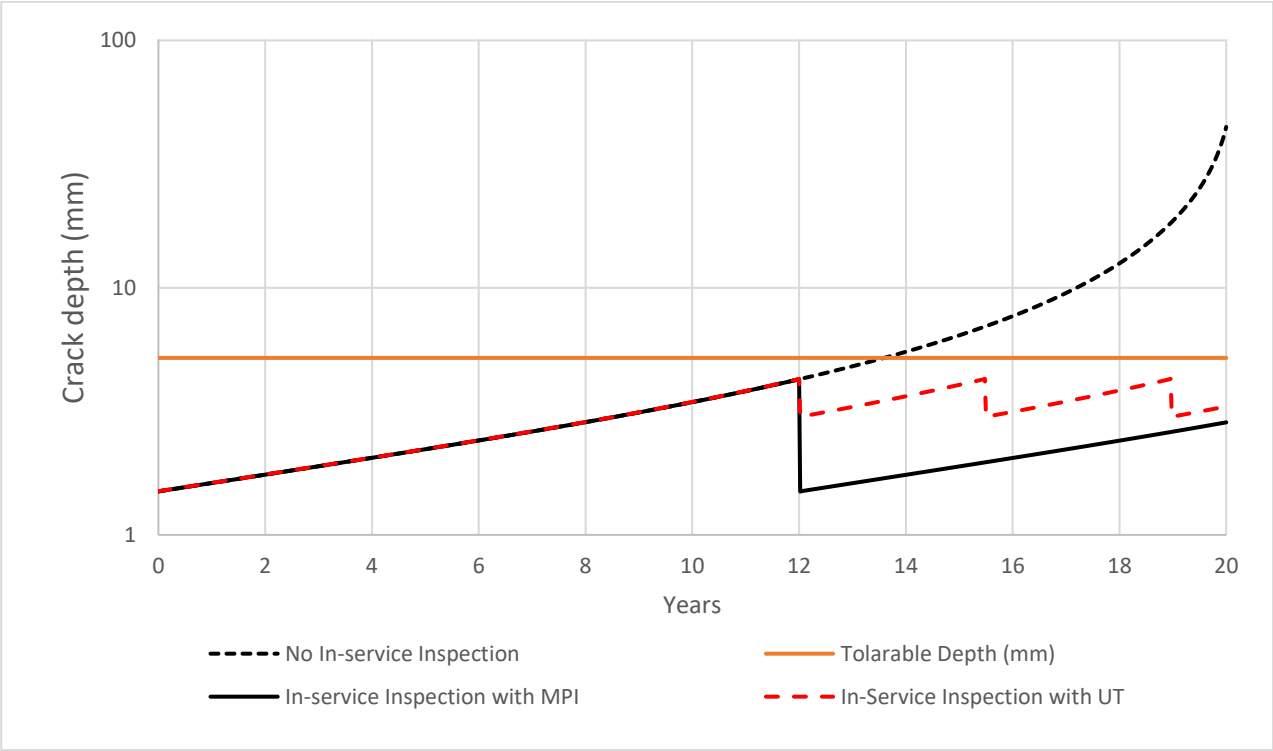


Figure 22 Effect of weld profile condition on in-service inspection

517 The effect of choice NDT for in-service inspection was studied by considering a case where UT is
518 chosen as the inspection method. The detection reliability specified in Table 1 used to determine
519 the crack size that can be left undetected after inspection. Figure 23 shows the predicted crack
520 size compared to inspection with MPI. It is observed that to keep the crack size below tolerable
521 size three inspections are required instead of one inspection using MPI.



522
523 **Figure 23 Selection of NDT method based on probability of detection and crack size at the time of inspection**

524 **5.2 Effect of environment**

525 In the event of insufficient corrosion protection, the fatigue crack growth will be accelerated.
526 The accelerated crack growth rate is reflected in fracture mechanics by changing the Paris law
527 constants to those observed in the corrosive environment. This is shown in Figure 24 and Figure
528 25, where the previously studied defect is assessed under a free corrosion environment instead
529 of the air environment. It is observed that failure is predicted to occur as early as 3.4 years after
530 commissioning. One strategy could be increased attention to the execution of corrosion
531 protection measures before commissioning. Additionally the joint should be inspected for the
532 signs of corrosion at least every three years.

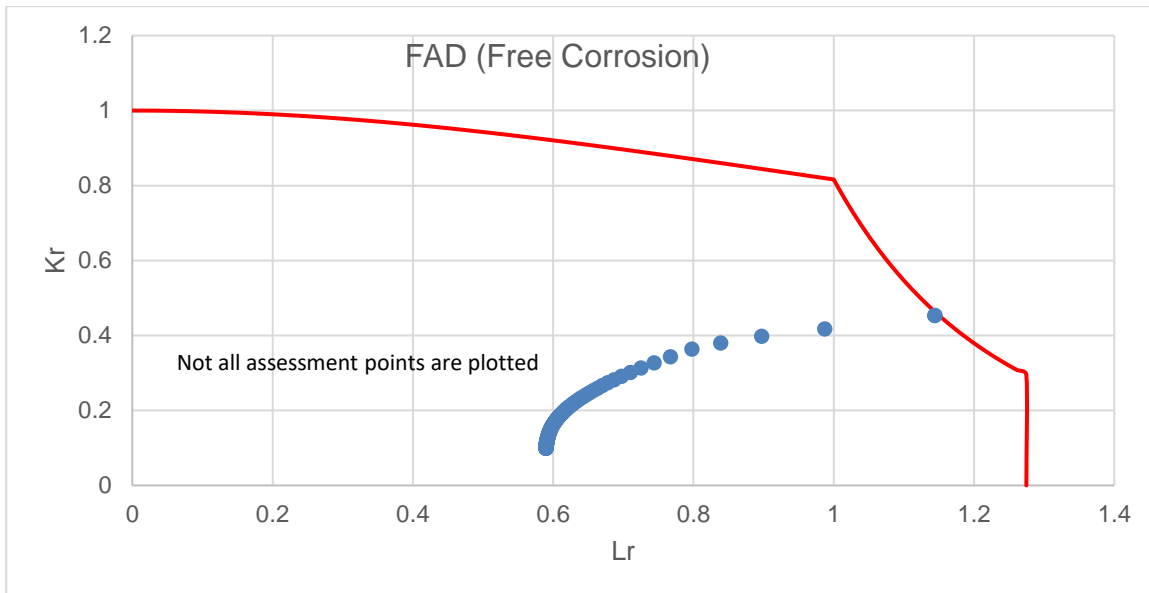


Figure 24 Failure assessment diagram (FAD) for crack growth in HAZ and with free corrosion

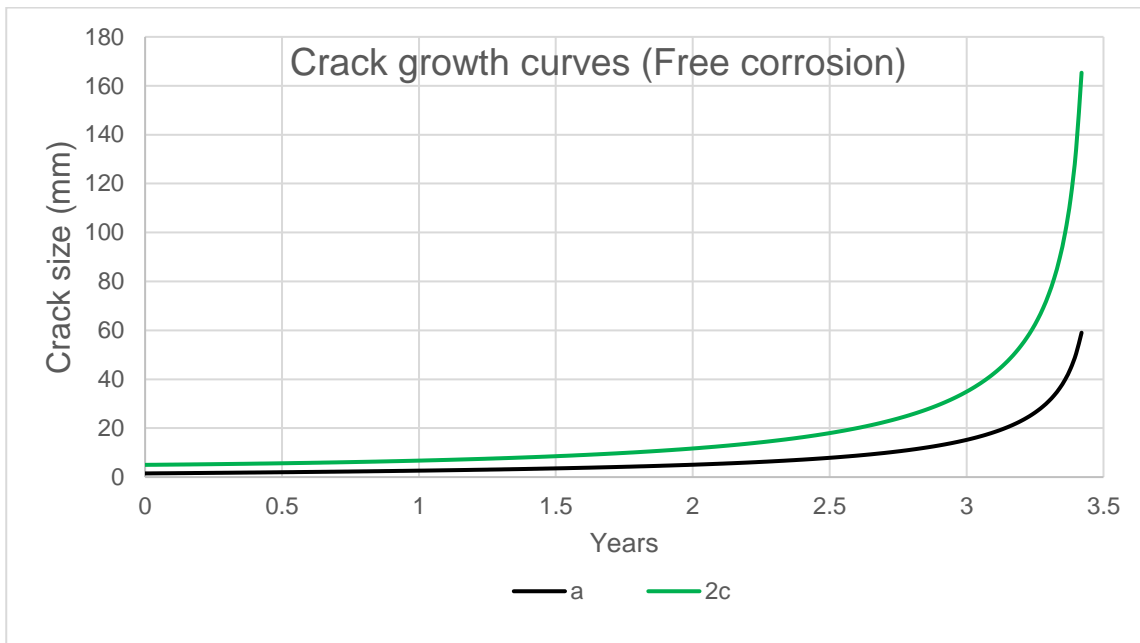


Figure 25 Crack growth curves for propagation in HAZ and with free corrosion

6 Case-Study 2: Probabilistic Fracture Mechanics application to a plate failure

Many structural members of offshore structures can tolerate cracks even after they become through-thickness. These structures may be idealised by plates containing through-thickness cracks (Figure 26). This can be for example for a less critical location of the structure in case-study 1 with lower stress levels.

Here, the application of probabilistic fracture mechanics to such a structure is demonstrated. The assumed inputs are listed in Table 7.

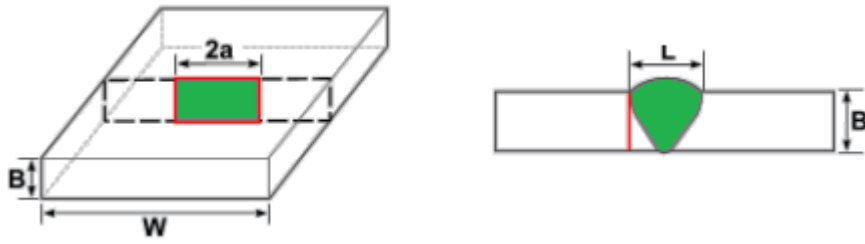


Figure 26 Through-thickness Crack geometry diagram

Case Description		
Case study structure	Offshore topside Platform with Long-term stress shape parameter = 0.85 and load cycle rate = 5.063 cycles/ min	
	Maximum design stress = 0.62 * Yield stress	
Material Properties	Young Modulus	210 MPa constant (Gentils et al., 2017)
	Poisson Ratio	0.3 constant (Gentils et al., 2017)
	Yield stress (σ_Y)	450 MPa constant (Gentils et al., 2017)
	Tensile strength	560 MPa constant (Gentils et al., 2017)
	Toughness	200 MPa* m ^{0.5} assumed
Fatigue assumptions	Crack growth model	Single slope Crack growth
	Cyclic stress	Equivalent constant amplitude stress 21 MPa
	Stress Intensity Solution	Through-thickness flaw in an infinite Plate
	Paris Law parameters	BS 7910 recommended values
	Design cycles in life	$N_{life} = \text{load cycle rate} \left(\frac{\text{cycles}}{\text{min}} \right) * (20 [\text{year}] * 365 [\text{day per year}] * [\text{hour per year}] * 60 [\text{min per hour}])$, for this structure = $5.322 * 10^7$
Fracture assumptions	FAD	BS 7910 Option 1
	Primary stress	A Weibull distribution with scale parameter 9.47 MPa
	Secondary stress	Weld Residual stress= Constant 100 MPa, assumed
	Thickness (B)	60 (mm) (Gentils et al., 2017)
	Initial Flaw dimensions (2a)	Exponential distribution with a mean value of 2 mm
Inspection Capabilities	In-service surface inspection	Surface inspection for ground welds above the water surface (Figure 11)

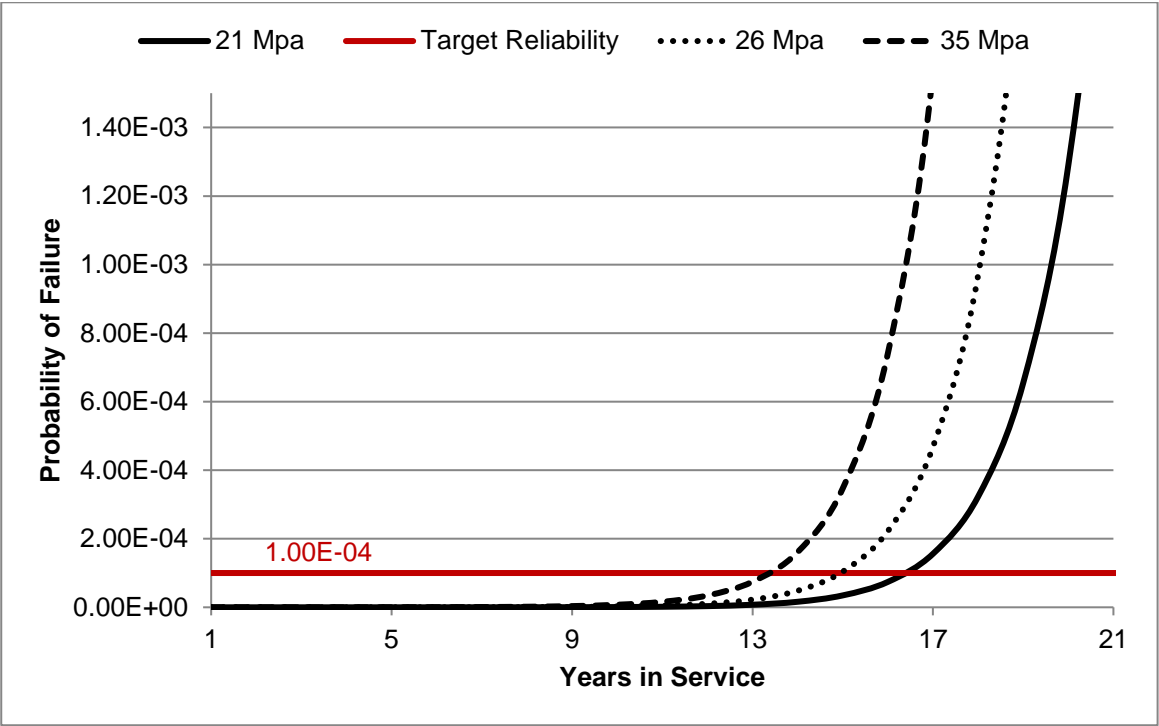
Table 7 Inputs for probabilistic Fatigue and fracture mechanics assessment

Figure 27 shows fatigue and fracture reliability of the structure under three levels of equivalent constant amplitude cyclic stress. As a starting point, 21 MPa cyclic stress which corresponds to the extreme stress of $0.62 \sigma_Y$ is selected. Target reliability level of 1.00×10^{-4} from Table 4 for Offshore Wind Turbines (unmanned structures) is selected. The structure will reach the target tolerable probability of failure just before year 17, suggesting that the structure should be inspected prior this time. As it is shown in Figure 28, such an inspection will reduce the failure probability below the target level for the rest of the intended service life.

If the aim was to design the structure to the safe-life design philosophy, the stress would have needed to be reduced below the current level. This, however, may not be an economical option since the current extreme stress level already possesses a significant safety factor ($0.62 * \sigma_Y$)

558 and reducing the stress will require bigger cross-sectional dimensions and, hence, a heavier and
559 more expensive structure. Integrating in-service inspection options in design can potentially
560 result in a more efficient design.

561 Furthermore, the design cyclic stress may be increased considering the availability of in-service
562 inspection. Two stress levels are considered here: An upper bound limit value of 35 MPa
563 corresponding to extreme stress equal to the Yield stress and a moderate value of 26 MPa. As
564 depicted in Figure 27, the probability of failure curve will be shifted to the left 2 and 3 years,
565 respectively. It is evident that the structure can sustain higher levels of stresses provided that
566 the appropriate time for inspection is determined and also other required limit states are not
567 violated.



568
569 **Figure 27 Fatigue reliability (FM) of a welded joint in an offshore structure for three different constant amplitude**
570 **stresses**

571 The effect of an inspection schedule is considered for the case of through-thickness crack under
572 21 MPa cyclic stress. It was shown previously in Figure 27 that, the structure is predicted to
573 reach the target tolerable probability of failure just before year 17, thus, the inspection should
574 be scheduled prior to this time. Here, a number of inspection options are considered.

575 Any inspection earlier than year 6 appears to have little benefit as the failure probabilities are
576 below 5.0E-8, a very low probability of failure. The reduction in the probability of failure is in
577 the order of one and the structure is likely to exceed the target level of reliability again close to
578 the final year of service. Inspection between year 10 to 15 shows the most effective results by
579 keeping the structure way below the target level throughout and to the end of service life
580 ensuring a considerable level of safety as well as providing further life extension possibilities in
581 the final years of designed service life.

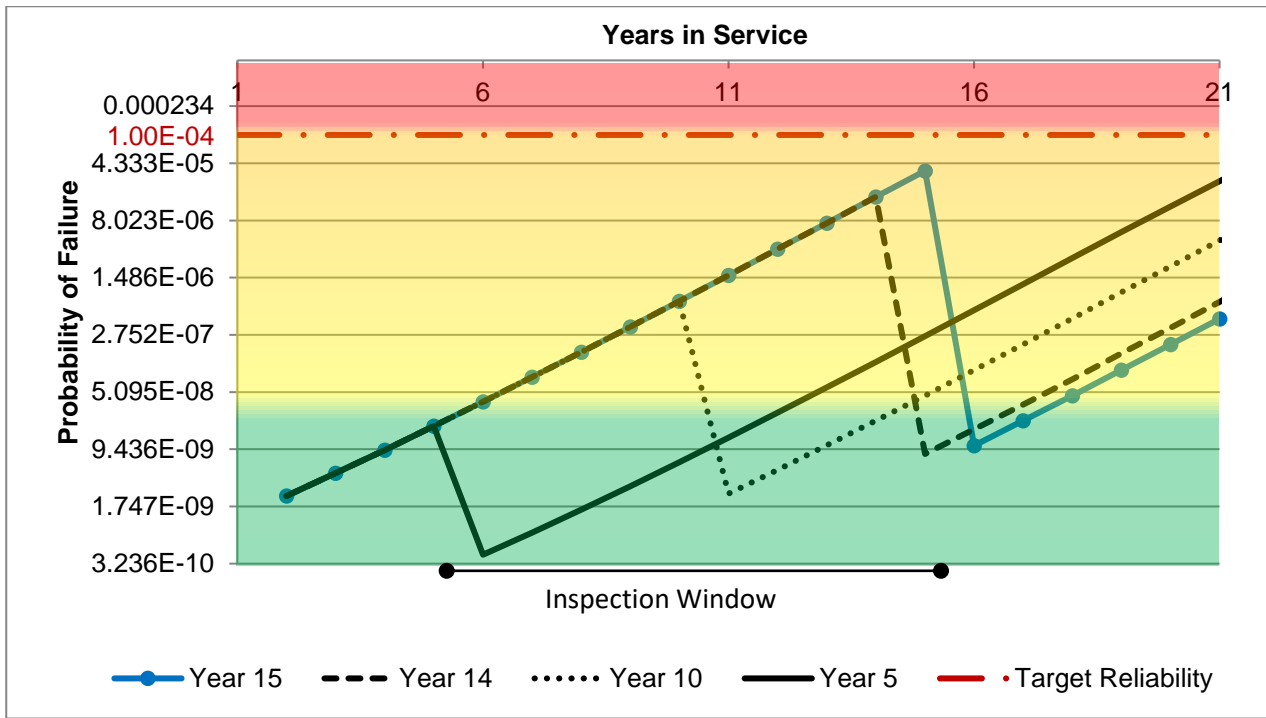


Figure 28 Crack growth curves of case study through-thickness in a plate considering different first inspection times

7 Conclusions

This paper presented a new approach to fatigue design of offshore wind turbine support structures. Traditionally, the design of offshore renewable structures against fatigue failure has been performed using the so-called S-N curve method. This approach, however, suffers from several limitations, such as limited ability to integrate the inspection capabilities. The structural design can significantly benefit from the inspectability of the structure by considering the damage-tolerant nature of many offshore structures. Fracture mechanics is a powerful tool capable of addressing a wide range of limitations associated with the S-N approach.

In this work, a framework for the design of offshore structures based on fracture mechanics was developed and its applications to a monopile wind turbine support structure were demonstrated. Additionally, the probabilistic fracture mechanics approach and its application in optimising in-service NDT inspection for a plated structure under sea wave loading was presented.

It was found that the design of the structure can be enhanced by specifying weld crown improvements which leads to better fatigue performance and reduced in-service inspection. The MPI will allow for thrice the inspection interval window than UT.

The probabilistic model showed to have the capability to account for uncertainty in design and inspection variables including NDT reliability. It also provides a likelihood of failure which can be used to calculate the risk associated with the chosen inspection time and in turn for optimising inspection using a, for example, cost-benefit analysis.

Additionally, the proposed optimisation model can be used for any practice of structural optimisation of OWT support structures

Authors contribution

PA conducted the research, created the proposed framework, performed all case study analysis, made the figures, and planned and wrote the paper. BF and AK contributed to the research with

608 intensive discussions and added to the paper with conceptual discussions and internal review.
609 AK secured the funding for this paper.

610 **Competing of interest**

611 The authors declare that they have no conflict of interest.

612 **Acknowledgements**

613 This work was supported by a grant from the Supergen Wind Hub EP/L014106/1, from the UK
614 Engineering and Physical Sciences Research Council (EPSRC), under the Flexible Funding
615 Scheme for University Strathclyde. Furthermore, this project has received funding from the
616 European Union's Horizon 2020 research and innovation program under grant agreement No.
617 745625 (ROMEO, 2019).

618 **References**

619 Amirafshari, P.: Optimising Non-destructive Examination of newbuilding ship hull structures
620 by developing a data-centric risk and reliability framework based on fracture mechanics,
621 University of Strathclyde., 2019.

622 Amirafshari, P. and Stacey, A.: REVIEW OF AVAILABLE PROBABILISTIC MODELS OF
623 THE CRACK GROWTH PARAMETERS IN THE PARIS EQUATION, in OMAE2019-961,
624 OMAE., 2019.

625 Amirafshari, P., Barltrop, N., Bharadwaj, U., Wright, M. and Oterkus, S.: A Review of
626 Nondestructive Examination Methods for New-building Ships Undergoing Classification
627 Society Survey, J. Sh. Prod. Des., 33(2), 1–11, 2018.

628 Anderson, T. L.: Fracture Mechanics: Fundamentals and Applications, 2005.

629 Arany, L., Bhattacharya, S., Macdonald, J. and Hogan, S. J.: Design of monopiles for offshore
630 wind turbines in 10 steps, Soil Dyn. Earthq. Eng., 92, 126–152,
631 doi:10.1016/j.soildyn.2016.09.024, 2017.

632 Ayyub, B. M., Akpan, U. O., Rushton, P. A., Koko, T. S., Ross, J. and Lua, J.: Risk-informed
633 inspection of marine vessels., 2002.

634 Barltrop, N. D. P. and Adams, A. J.: Dynamics of fixed marine structures, Butterworth-
635 Heinemann., 1991.

636 Baum, S., Von Kalben, C., Maas, A. and Stadler, I.: Analysis and Modelling of the Future
637 Electricity Price Development by taking the Levelized Cost of Electricity and large Battery
638 Storages into Account, 2018 7th Int. Energy Sustain. Conf. IESC 2018, 1–8,
639 doi:10.1109/IESC.2018.8440005, 2018.

640 Bertsche, B.: Reliability in automotive and mechanical engineering: determination of
641 component and system reliability, Springer Science & Business Media., 2008.

642 Bhattacharya, B., Basu, R. and Ma, K.: Developing target reliability for novel structures: the
643 case of the Mobile Offshore Base, Mar. Struct., 14(1–2), 37–58, 2001.

644 British Standard: BS 7910:2019, Br. Stand. Institutions, London, 2019, 2019.

645 BS7910, B. S.: BS 7910:2013+A1:2015 AnnexJ, 2015.

646 BSI: BS EN 1990: 2002+ A1: 2005--Basis of Structural Design, 2005.

647 BSI7608: Guide to fatigue design and assessment of steel products, London BSI Stand. Publ.,
648 2015.

649 Da Costa, L. M., Danziger, B. R. and Lopes, F. D. R.: Prediction of residual driving stresses in
650 piles, *Can. Geotech. J.*, 38(2), 410–421, doi:10.1139/cgj-38-2-410, 2001.

651 DNV: Structural reliability analysis of marine structures, Det Norske Veritas., 1992.

652 DNV: Fatigue design of offshore steel structures, No. DNV-RP-C203, 2010.

653 DNV: Design of offshore wind turbine structures, DET NOR SKE Verit., 2013.

654 DNV: DNVGL-RP-C210-Probabilistic methods for planning of inspection for fatigue cracks in
655 offshore structures, 2015.

656 DNVGL: DNVGL-ST-0126: Support Structures for Wind Turbines, Oslo, Norw. DNV, 2016a.

657 DNVGL: DNVGL-ST-0437 Loads and site conditions for wind turbines., 2016b.

658 European Environment Agency: Share of EU energy consumption from renewable sources,
659 2005–2050., 2019.

660 Førli, O.: Guidelines for Development of NDE Acceptance Criteria, Nordtest., 1999.

661 Fraile, D., Komusanac, I. and Walsh, C.: Wind energy in Europe: Outlook to 2023., 2019.

662 Gentils, T., Wang, L. and Kolios, A.: Integrated structural optimisation of offshore wind
663 turbine support structures based on finite element analysis and genetic algorithm, *Appl.*
664 *Energy*, 199, 187–204, 2017.

665 Georgiou, G. A.: Probability of Detection (POD) curves: derivation, applications and
666 limitations, Jacobi Consult. Ltd. Heal. Saf. Exec. Res. Rep., 454, 2006.

667 Hobbacher, A. F.: Recommendations for Fatigue Design of Welded Joints and Components,
668 Springer International Publishing, Cham., 2016.

669 HSE: HSE's decision-making process, edited by HSE, HSE., 2001.

670 IEC: 61400-3 (2009) Wind Turbines—Part 3: Design Requirements for Offshore Wind
671 Turbines, 2009.

672 IEC: BS EN IEC 61400-1: Wind turbines part 1: Design requirements, Int. Electrotech.
673 Comm., 2019.

674 ISO-14971: BS EN ISO 14971: 2012—Application of risk management to medical devices,
675 2012.

676 ISO-31000, B. S.: 31000,(2018) Risk management--Principles and guidelines, Int. Organ.
677 Stand. Geneva, Switz., 2018.

678 Jonsson, B., Dobmann, G., Hobbacher, A. F., Kassner, M. and Marquis, G.: IIW Guidelines on
679 Weld Quality in Relationship to Fatigue Strength, Springer International Publishing, Cham.,
680 2016.

681 Lassen, T. and Recho, N.: Fatigue life analyses of welded structures: flaws, John Wiley &
682 Sons., 2013.

683 Li, L., Moan, T. and Zhang, B.: Residual stress shakedown in typical weld joints and its effect
684 on fatigue of FPSOs, in ASME 2007 26th International Conference on Offshore Mechanics and

685 Arctic Engineering, pp. 193–201., 2007.

686 Lotsberg, I., Sigurdsson, G., Fjeldstad, A. and Moan, T.: Probabilistic methods for planning of
687 inspection for fatigue cracks in offshore structures, *Mar. Struct.*, 46, 167–192, 2016.

688 Luengo, M. M. and Kolios, A.: Failure mode identification and end of life scenarios of offshore
689 wind turbines: A review, *Energies*, 8(8), 8339–8354, doi:10.3390/en8088339, 2015.

690 Mehmanparast, A., Brennan, F. and Tavares, I.: Fatigue crack growth rates for offshore wind
691 monopile weldments in air and seawater: SLIC inter-laboratory test results, *Mater. Des.*, 114,
692 494–504, 2017.

693 Naess, A.: Fatigue handbook: offshore steel structures, 1985.

694 Okumoto, Y., Takeda, Y., Mano, M. and Okada, T.: Design of ship hull structures: a practical
695 guide for engineers, Springer Science & Business Media., 2009.

696 ROMEO: ROMEO, [online] Available from: <https://www.romeoproject.eu/>, 2019.

697 Tavner, P.: Offshore wind turbines: Reliability, availability and maintenance., 2012.

698 twd: Monopile Fabrication, [online] Available from: [https://twd.nl/suction-bucket-jacket-](https://twd.nl/suction-bucket-jacket-seafastening-structures/suctionbucketjacket_seafastening_clamps_overview/)
699 [seafastening-structures/suctionbucketjacket_seafastening_clamps_overview/](https://twd.nl/suction-bucket-jacket-seafastening-structures/suctionbucketjacket_seafastening_clamps_overview/), 2019.

700 TWI: Structural Integrity Assessment and Practical Application of BS 7910 Procedures for the
701 Assessment of Flaws in Metallic Structures., 2015.

702 Van Wingerde, A. M., Van Delft, D. R. V., Packer, J. A. and Janssen, L. G. J.: Survey of
703 support structures for offshore wind turbines., 2006.

704 Zerbst, U., Klinger, C. and Clegg, R.: Fracture mechanics as a tool in failure analysis—
705 Prospects and limitations, *Eng. Fail. Anal.*, 55, 376–410, 2015.

706